Vein Visualisation: Development of a Non-Contact Vein Visualisation System

Robert Brennan, BSc

University College Dublin

School of Electrical and Electronic Engineering

May 2016

The thesis is submitted to University College Dublin in part fulfilment of the requirements for the degree of

Master of Biomedical Engineering

Doctor James Ryle	Principal Supervisor
Professor John Sheridan	Principal Supervisor
Professor Madeleine Lowery	Programme Coordinator
Doctor Andrew Keane	Head of School

Acknowledgements

I would like to thank Dr. James Ryle for his invaluable contribution to both my project and professional development. I would also like to thank Prof. John T.Sheridan for his encouragement and advice throughout my project.

Thanks to the UCD optical engineering department for accommodating me within the laboratory environment. I also want to thank the volunteers who contributed test data to evaluate the performance of the final system.

My family and friends have helped me throughout my time in UCD. Without their constant support this would not have been possible and I will always be grateful. Thanks for all the dinners, lifts, motivation, advice and laughs.

Abstract

A number of physiological processes within the human body cause imperceptible changes in the environments around them. Techniques have been developed to capture these changes using imaging devices, allowing them to be both visualised and measured. In this paper, a system was built to image subcutaneous veins using a technique called near infrared imaging. It involves exploiting the ability of near infrared light (700 nm – 1000 nm) to penetrate further into the body and allows high contrast images of the blood vessels to be obtained. Experiments were carried out to determine the point on the near infrared spectrum at which the highest contrast between the blood vessels and surrounding tissue could be observed. An 850 nm light source was found to produce the highest contrast between the tissue and the surrounding blood vessels.

In order to further improve the diagnostic capability of the technology, two other imaging techniques were implemented within the system; laser speckle imaging and Eulerian video magnification. Laser speckle imaging was used to detect regions of haemodynamic flow. It was demonstrated that the technique could be used to detect regions of blood flow underneath the skin. Similarly, Eulerian video magnification, a video processing technique was implemented within the system which was used to extract a heart rate signal. Tests were developed to determine how accurately this signal could be extracted from near infrared videos. Using this method to extract heart rate, average error was reduced from 15.6% at 650 nm to only 3.48% when an 850 nm light source was used.

List of Tables

List of Figures

Nomenclature

All symbol and abbreviations are declared at the point of first appearance within the text. They are listed below for convenience and contain the section in which they are first declared.

NIR	Near infrared, Section 1
EVM	Eulerian Video Magnification, Section 1
LSI	Laser Speckle Imaging, Section 1
LED	light emitting diode, Section 2.1
I_{skin}	Intensity value recorded in a region containing skin, Eqn.1
I_{vein}	Intensity value recorded in a region containing a vein, Eqn.1
n	The bit depth of the captured images, Eqn. 1
S	The size of each speckle speckle grain in the Speckle field, Eqn. 2
λ	The wavelength of light, Eqn. 2
$F_{\#}$	The focal number of a lens, Eqn. 2
M	Lens Magnification, Eqn. 2
BPM	beats per minute, Section 2.1

Table of Contents

1. Introduction

Imaging the human body and extracting signals from the physiological processes within can present significant difficulties. The limitations of established systems generally fall into three categories: cost, safety and efficacy. Other established imaging systems, like ultrasound, tend to require skilled technicians to operate properly and require highly specialised equipment. This project will explore and attempt to minimise the effect of these three limitations in the development of a non-contact vein visualisation device.

Vein visualisation and non-contact biological signal extraction is important in a clinical context. Continuous failed vein access attempts are associated with pain, infection and reduced ability to administer important treatments in long term patients [1]. Different solutions have been developed to improve the ability of healthcare providers to access the blood vessels. Implantable devices have been used to provide access to a particular vein but tend to increase medical complications. They require a surgical procedure to be implanted within the body, and increase the risk of patient infection. In a trial on a group of 250 patients, 10% contracted an infection as a result of the implantable devices but only 2% reported that day to day discomfort was increased [2]. Another suggested solution involves employing an imaging device to visualise the blood vessels. A number of devices have been approved by the FDA to perform exactly this purpose.

AccuVein and *Veinlite* both produce the most widely implemented commercially available products used to assist in accessing the blood vessels. The devices they produce, however, have varied reports of success. Some studies have reported first

attempt vein access rates increased by as little as 2% [3]. The *AccuVein AV300* vein visualisation device typically retails at £2,900 in the UK [4]. This cost is significant if the expected benefits are low.

The *AccuVein* vein visualisation devices capture images of the human body in the near infrared (NIR) spectrum of light. Less NIR light is absorbed by the skin, allowing it to penetrate further into the body. However, the NIR absorption characteristics of the skin have been found to vary significantly with varying concentrations of melanin, the pigment associated with skin colour [5]. This could be a possible explanation as to why darker skin patient groups tend to experience more difficulty in using vein visualisation devices.

Another hindrance to NIR vein visualisation technology relates to the limited information it provides. Only the position of the blood vessels can be determined. Devices on the market provide no insight into relevant characteristics typically considered while trying to insert a needle; Vessel depth, diameter and rate of blood flow [6].

In this respect, other methods have been developed which are capable of obtaining this important information and use similar equipment to NIR imaging systems. Laser Speckle Imaging (LSI) involves analysing variations within the interference pattern created by coherent laser light. It has been used before in laboratory settings to determine bone fractures in animal trials [7] and to study cerebral blood flow in exposed rodent brains [8].

Similarly, a video processing technique [9] designed to exaggerate movement within videos was able to amplify skin colour change so that a pulse signal could be extracted.

The technique, named Eulerian Video Magnification (EVM), would not require changes to equipment within the system, allowing it to be implemented at a low cost.

The quality of the results obtained using NIR vein visualisation depend on a variety of factors which are cited within related literature. Skin colour [10], Age [11] and body fat percentage [12] have all been mentioned as limiting factors within trials attempting to implement vein visualisation devices in real world settings.

Akbari *et al* used pig skin samples to study the penetrative depth of NIR light in the body [13]. The work showed that there was a relationship between observed light intensity and blood vessel depth. However, the characteristics varied significantly between different samples.

The main aim of this research is to develop a cheap, non-contact vein visualisation device. This project will also attempt to identify the optimal wavelength at which to visualise the veins. It will explore EVM and LSI in an effort to develop a device with increased diagnostic ability compared to established vein visualisation devices.

2. Background and Literature Review

Modern imaging devices are capable of picking up details which are imperceptible to the human eye. In the following chapter it will be shown how image processing techniques have been used to amplify these tiny details to make it possible to extract a variety of useful signals. In particular, research has been conducted into how they can be implemented within the medical device industry. Extracting biological signals from patients without touching them could help to reduce infection rates and improve patient care.

A single imaging system, properly utilised, could be used to extract signals from the body at a fraction of the cost of traditional medical diagnostic equipment. Amplifying colour changes and movement using inexpensive imaging equipment can make it possible to visualise everything from heart rate to the blood vessels themselves. This chapter will examine the development of three particular branches of work in biomedical optics. Laying the ground work will help to identify the limiting factors of the technologies implemented to date and set a clear focus for future work within the field.

2.1 Eulerian Video Magnification

A team of researchers in MIT [9] developed a simple video processing technique which could be used to make imperceptible changes in the world visible. The technique, called Eulerian Video Magnification (EVM), involves amplifying temporal frequency bands to enhance low amplitude, low frequency changes within the video of interest. They used EVM in particular to amplify the temporal frequencies

corresponding to normal heart rate (0.5 Hz – 4 Hz) [14]. The normally invisible change in skin tone as a result of pulsatile blood flow could be visualised and a heartbeat signal extracted. The signal and noise characteristics are important to consider. The effect of noise in the amplification of small amplitude signals has been investigated by one of the researchers involved in the original publication of EVM [15]. Guttag *et al* demonstrated the effect of acquisition noise on motion amplification, highlighting a number of factors that contribute to signal error. In particular, the similarity between the range of frequencies corresponding to movement and heart rate present a noteworthy problem. Removing movement artefacts has the potential to corrupt the signal of interest. This restricts the application of the method in real world settings where movement is impossible to avoid.

One of the exciting aspects of this video processing method is the fact that only a webcam and standard computer are required to implement the technology. The examples demonstrated by Wu *et al* in the original paper are produced under optimal conditions and do not attempt to address the issues associated with motion and dynamic lighting conditions corrupting the signals of interest.

Developing on the original EVM algorithm, another research team was able to improve the accuracy of heart rate estimation [16]. The original work required that the subjects remain still in the video frame. Alzahrani *et al* pre-processed video input by employing algorithms to reduce motion and identify and track facial features. EVM was then applied only to regions where the signal was likely to occur and not to the entire frame of each image. The error in signal estimation was reduced as a result from 9.7 beats per minute (BPM) to 6.12 BPM when compared to a hospital grade

heart monitor. The work emphasized the need for EVM to develop and become more robust to allow it to be implemented in a clinical environment.

Exaggerating the movement of the blood vessels themselves using Video Processing techniques could help to determine if a target vessel is suitable for vein access. During cannulation procedures it would be invaluable to have a system which could identify blood vessels and reduce failed vein access attempts. EVM has been used in tests on animal subjects in an effort to sufficiently exaggerate blood vessel movement for the purposes of automatic vessel identification [17]. A green light source was used as an illumination source, chosen to maximise the absorption of the light by the red blood cells. They enhanced contrast of the captured images and extracted binary skeletons of the underlying microvasculature. EVM was then applied to the series of captured images in an effort to exaggerate vessel motion and aid in vessel identification. Liu *et al* were able to implement the system to work automatically and in near real time, overcoming extended processing time which had been mentioned as a limitation in other research studies. The system they created focussed on visualising microvasculature and had to be placed against the skin. It demonstrates that EVM could be used to enhance existing vein visualisation technology but the system could not be used at any distance from the subject, limiting its use.

This study brings in illumination as an important aspect to EVM and similar techniques. Aliasing can distort the beat signal if the camera used is incapable of sampling at twice the frequency of the light source, as specified by the Nyquist sampling theorem [18]. Liu *et al* used a green light emitting diode (LED) as the sole source of illumination to overcome this issue (LEDs operate in DC) [17]. Other

implementations have used NIR LEDs as a light source in combination with a camera sensitive only to the NIR spectrum (750 nm – 950 nm). In one case the described system was used to monitor a truck driver's heart rate under dynamic lighting conditions [19]. Removing any light sources not operating at DC produced favourable results. It was reported that under dynamic lighting conditions the system had a maximum error of only 5.8 BPM. The particular method of extracting heart rate involved measuring the change in skin reflectivity as blood is pumped through the body, a technique called plethysmography. The use of NIR light within this work, however, is of interest and could be used to compliment EVM.

Applying EVM to NIR videos could reduce the noise amplified within the simple system and reduce the effect of uneven and uncontrolled lighting as a problem in heart rate extraction.

2.2 Near Infrared Imaging

NIR light is absorbed less by melanin in the skin and can, as a result, penetrate further into the underlying tissue. NIR imaging has been used to a limited extent in the area of vein visualisation. The band of light is reflected less by haemoglobin in the blood stream in comparison to surrounding tissue [5]. This allows high contrast images to be obtained of subcutaneous veins where blood vessels appear much darker in comparison to the surrounding tissues.

In one study conducted on the efficacy of commercial vein visualisation devices in a clinical context it was found that the technology consistently improved the phlebotomist's rate of successful vein access attempts [10]. It was found that in 62%

of cases at least one additional vein suitable for cannulation could be identified. It did, however, highlight potential patient characteristics hindering the ability of NIR imaging to identify veins like age and skin colour.

In a similar study on the efficacy of vein visualisation devices in children, it was found that the effective visualisation depth was reduced when visualising smaller blood vessels [11]. Cuper *et al* found that blood vessels with a diameter of 3.6 mm could be visualised to an average depth of 5.6 mm compared to a depth of 2.6 mm for vessels 1 mm thick. First attempt venepuncture failure was reduced using vein visualisation technology from 15% to only 2%. The study evaluated different wavelength light sources using a contrast ratio and found that 850 nm – 900 nm appeared to produce the highest contrast images. In both studies certain patient groups were demonstrated to benefit from the technology but highlighted the need for improvements to benefit difficult patients.

NIR imaging in literature is generally compared to alternative technologies like ultrasound and thermal imaging which can be used to derive information about the blood vessels. NIR imaging is cheaper to implement in general but it is thought of as somewhat less effective. NIR imaging is still incapable of determining anything but the vessels location and as a result has achieved less widespread implementation. There have been cases, however, where NIR imaging has been used in combination with ultrasound to augment the high contrast images with the haemodynamic characteristics of the vessel [20]. Ultrasound was also used to determine if the measured intensity of the blood vessels imaged using NIR imaging was proportional to blood vessel depth. The research conducted found that while a relationship between

vessel depth and recorded intensity did exist, it was by no means reliable, due to variance across human subjects and the complex nature of each layer of skin.

One of the main advantages of NIR imaging is that it is low cost and requires generally inexpensive equipment. In comparison Ultrasound requires a skilled technician to operate properly. In long term patients requiring frequent vein access an improved method of accessing veins could reduce rates of stenosis and infection. This would represent a combined benefit to healthcare facilities and patient quality of life. Patients could easily access veins with a reduced risk of damaging blood vessels.

There are some limitations to creating low cost NIR vein visualisation systems. In particular, an attempt to develop a prototype using a standard smart phone with a camera found that an external camera was required to drive the system [12]. This is because most commercially available cameras contain NIR filters which remove light from the spectrum of interest. It was shown that a standard webcam, with some minor modifications, was capable of obtaining NIR images. They found that in a small clinical study the prototype, using a standard USB camera and a mobile phone to process the images, performed with similar efficacy to more expensive commercial systems. Similar to Shahzad *et al* on average 1.6 additional veins were detected by clinical staff using the system [20]. This expands the potential uses of NIR imaging beyond a purely clinical environment and demonstrates that NIR imaging systems can and should be inexpensive to implement.

The use of NIR imaging to augment surgical procedures has also been suggested [13]. Akbari *et al* highlighted the need for a simple and effective way to distinguish between arteries and veins during surgical procedures. They demonstrated a method where

NIR spectrometry was used to find unique spectral signatures between the arteries and veins. They found that the highest spectral difference between the two types of blood vessels was found to lie between 600 nm – 700 nm. This is based however on the assumption that the veins are exposed during surgery. It is recognised that haemoglobin and deoxyhaemoglobin have, in the same way, different spectral characteristics in the NIR spectrum. It is suggested that NIR imaging could be applied to characterise blood vessels before surgery, thus reducing overall operating time.

Other work carried out used NIR imaging to monitor brain tissue oxygen concentration [21]. They were able to distinguish the brain activity of two cognitive activities by measuring the NIR spectral changes in tissue oxygenation. This work, while basic, shows with additional research NIR imaging could become a very powerful diagnostic tool.

NIR imaging appears to have the potential to overcome many of the limitations of EVM. NIR imaging could allow EVM to be applied to structures underneath the skin, thus reducing amplified noise and hence the effectiveness of physiological signal extraction.

2.3 Laser Speckle Imaging

The final technique to be examined as an alternative method of extracting biomedical signals is LSI. LSI involves shining coherent laser light onto a rough surface to generate a random interference pattern. It has been found that the interference or speckle pattern is statistically normal when the surface is static but exhibits a change in the statistical properties when the surface is dynamically changing [22]. This

property of laser speckle interference patterns has been exploited to determine information about sub-cutaneous fluid flow.

There are a number of algorithms which have been used to differentiate static and dynamically moving regions within the imaged speckle fields. They either exploit the spatial or temporal properties of the speckle field [23]. Ansari *et al* were able to use spatial LSI to detect increased blood flow in the hand after applying a force, demonstrating the capabilities of the technique to detect movement underneath the skin [24]. They concluded the work by noting that spatial LSI produced less resolved detail when compared to temporal LSI alternatives, but required lower processing times to produce results.

This identifies that a trade-off has to be made between resolution and speed of acquisition but outlines the potential for aspects of each algorithm to be combined to achieve optimal results for the particular application.

In recent studies, the light source used to generate the laser speckle pattern has been investigated with respect to measuring human blood flow. Initial results using pig skin samples demonstrated that speckle patterns generated using NIR laser light were more sensitive to dynamic changes caused by blood flow in comparison to visible light [25]. They used pig skin samples of varying thickness to show that there was a relationship between the intensity of the measured speckle pattern and the thickness of the skin sample. It was interesting to note that they determined that the speckle pattern fluctuates temporally in direct proportion to blood flow within the sample. This study shows that LSI, similar to EVM, can be enhanced by NIR imaging in biological applications. Using LSI to measure blood flow, it would be expected that the speckle

pattern would blur in proportion to the rate of flow underneath the skin surface. There is the potential for EVM to amplify the temporal statistical changes caused by dynamic movement underneath the skin in order to enhance the output contrast.

In other work attempting to analyse cerebral blood flow an alternative method of LSI is outlined which involves estimating and removing static elements of the interference pattern [8]. It was found to produce images with higher contrast between static regions and areas with blood flow. It also prevents surface glare from the samples which dramatically reduces error within the images obtained. The work demonstrates that the standard equations used to determine laser speckle contrast have room to develop and LSI holds the potential to become a powerful tool with respect to medical imaging.

In contrast to NIR imaging, LSI is typically performed using expensive scientific grade monochrome cameras. It has been demonstrated, however, that similar results when imaging blood flow using speckle patterns can be obtained using cheaper commercial colour cameras [26]. Yang *et al* demonstrated that the camera used had to allow manual control over a number of settings including shutter speed and aperture size but as long as these requirements were met, the overall result was the same. With this in mind, LSI can be performed at a relatively low cost and potentially with the same equipment required to implement NIR imaging.

LSI has been used in a variety of other medical applications. It has been used as an alternative method of detecting broken bones within the body. A standard laser speckle pattern was used to illuminate the surface of a chicken subject and a loudspeaker was introduced to induce vibrations within the chicken's limb [7]. While the results were preliminary it was demonstrated that broken bones could be detected

in the chickens with a 90% accuracy. If this could be implemented eventually in humans, it could be used to reduce the number of x-rays required and avoid excessive exposure to dangerous x-rays.

LSI, NIR and EVM all have one thing in common; they exaggerate details imperceptible to the human eye. LSI and EVM have both been shown to benefit from being performed in the NIR spectrum. In the same vein, methods demonstrated to improve the effectiveness of NIR imaging could have the potential to enhance the effectiveness of the other mentioned techniques as well. Chemicals which are biologically inert and fluoresce in the presence of NIR light have been used to improve the contrast of NIR vein visualisation systems [27]. Shimada *et al* demonstrate the improved visualisation of blood flow during a number of surgeries using indocyanine green. The fluorescing agent was used to evaluate the effectiveness of organ reconstruction and reduce anastomotic leakage. It could also be used to visualise the delivery of particular drugs within the body. In another study the same contrast agent was used to enhance NIR imaging to such an extent that it could be used to identify hepatoblastoma, malignant tumours within the liver [28]. The only problem identified with the system in this case was that only tumours closer to the surface could be correctly identified.

2.4 Diagnostic Potential of a Combined System

NIR imaging, LSI and EVM have not seen widespread clinical implementation to date. The three techniques have developed significantly and with recent technological

advances to date the associated costs are relatively low in comparison to other established devices able to carry out similar tasks.

Making the technology more automatic and less prone to user error is critically important in stimulating commercial demand for the technology. The similarities between the three methods show that combining them together could be done relatively easily and potentially produce a more robust imaging system. It has already been shown that EVM and LSI benefit when NIR light is used as the governing light source.

Other interesting solutions have been found to improve the potential of NIR imaging even further by using fluorescing agents which could be expected to similarly improve EVM and LSI. It is apparent from available research that there is no consensus on the particular parameters that should be used for the chosen imaging equipment or the exact wavelengths of the selected light source. It is highlighted repeatedly that natural human variation require that these variables remain as flexible as possible in order to accommodate a wider range of patients.

3. Methods

This chapter details the key steps in the development of the proposed vein visualisation device. It illustrates the design choices made while selecting a number of the key components and describes the steps taken to perform three tests used to assess system performance.

3.1 System Design

A configurable testing device was developed in order to demonstrate and test the capabilities of NIR imaging, LSI and EVM. The system described in Figure 1 is made up of three main components; (i) an LED array, capable of emitting light at a range of wavelengths, (ii) an infrared laser and (iii) an image sensing system.

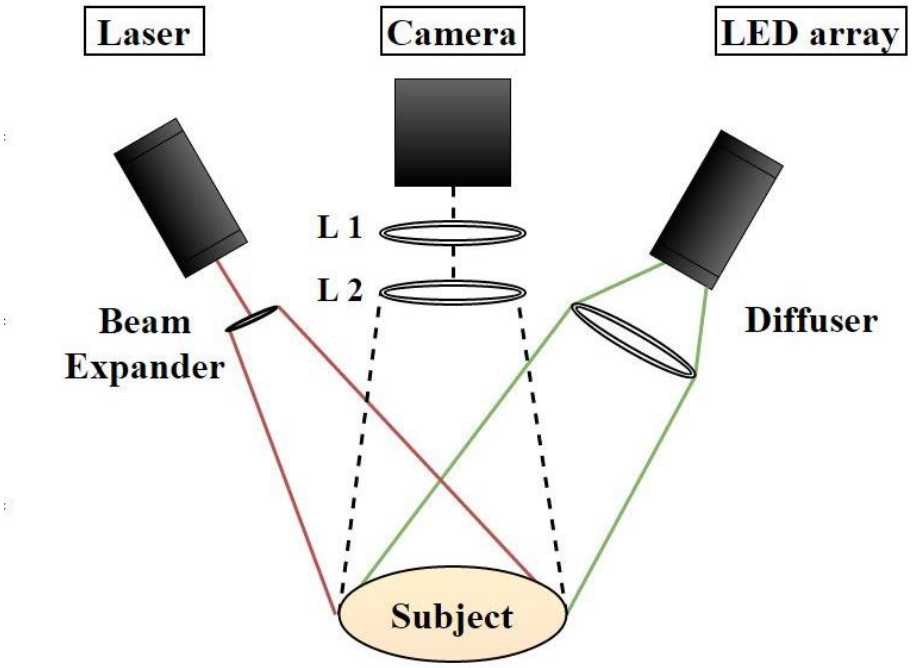

Figure 1. Schematic of proposed vein visualisation system

3.1.1 Selecting a Suitable Image Sensor

The camera model was an important design choice. A balance between cost and efficacy had to be achieved to, at the very least, compete with existing vein visualisation systems. A Basler ACE ac640-750us model was chosen for a number of important factors; frame rate, cost and sensitivity. The camera is capable of capturing images at speeds of up to 750 frames per second (fps) which is vital to properly perform LSI. The camera is also supplied without an infrared filter allowing NIR images to be captured without any modification to the camera. Software was written in C++ using the Basler camera api to allow full control over the cameras features and to allow for maximum frame rates to be achieved.

ACE ac640-750us Camera Specifications	
Resolution (H x V pixels)	659 px x 495 px
Pixels Size (horizontal / vertical)	7.4 μm x 7.4 μm
Frame Rate	750 fps
Pixel Bit Depth	8 bits

Table 1. ACE ac640-750us Camera Specifications

Table 1 shows the chosen cameras specifications and a number of the parameters taken into account while designing different aspects of the system.

3.1.2 Safety Considerations

Safety was of utmost importance within the system design. NIR light delivers less energy than light of lower wavelengths. It is, however, invisible to the naked eye and does not elicit a blink response. This makes eye safety more of a concern. The relevant

regulations for LED and laser light were consulted and the illumination powers were kept below hazardous levels. IEC 60825 [29] and ANSI-Z136 [30] were both checked while determining illumination powers of the LED and laser light sources used within the final system. During testing, eye protection was provided to all test subjects and light exposure was limited by keeping test durations to a minimum.

3.2 NIR Imaging System

The following section describes the system built to perform NIR imaging and the test procedures used to verify the technology.

3.2.1 Development of NIR Imaging System

NIR imaging requires both a NIR sensitive camera and a NIR light source. In order to determine the optimal wavelength at which to capture images of sub-cutaneous blood vessels a configurable LED array was mounted onto the testing rig. Figure 2 illustrates the absorption coefficient of fat, water, deoxygenated blood and oxygenated blood at different wavelengths along the light spectrum [31].

It gives a general idea of the wavelengths which have the potential to best visualise the blood vessels. It is clear that between 800 nm and 900 nm the absorption coefficient of deoxygenated blood reaches a low point, highlighting a range within the NIR spectrum at which the veins will exhibit high contrast to surrounding tissue.

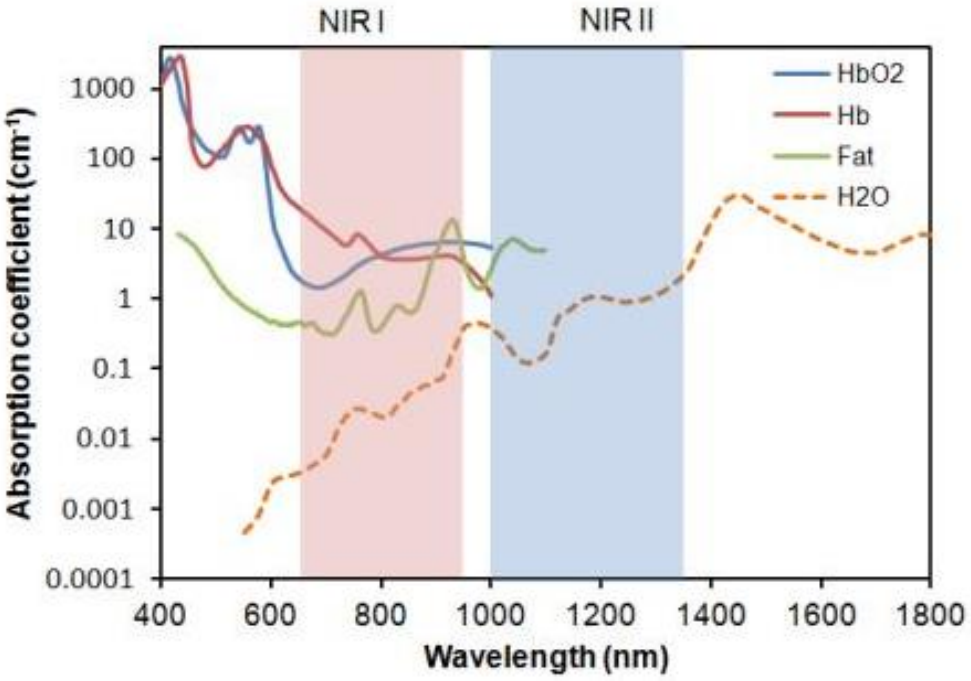

Figure 2. Absorption coefficient of oxygenated blood, deoxygenated blood, adipose tissue and water as a function of light wavelength

Four LED arrays were designed to represent different points within this range; 830 nm, 850 nm, 890 nm and 950 nm. A fifth LED array, emitting light at a peak wavelength of 650 nm, was made to represent the visible spectrum of light and highlight the ability of NIR light to capture images of subcutaneous blood vessels. A diffuser was placed in front of each LED grid to produce an even illumination pattern. Figure 3 describes the NIR imaging system and the placement of the camera and light source. The LED lighting was placed above the subject to reduce uneven illumination and scattering of light striking the skin at an angle.

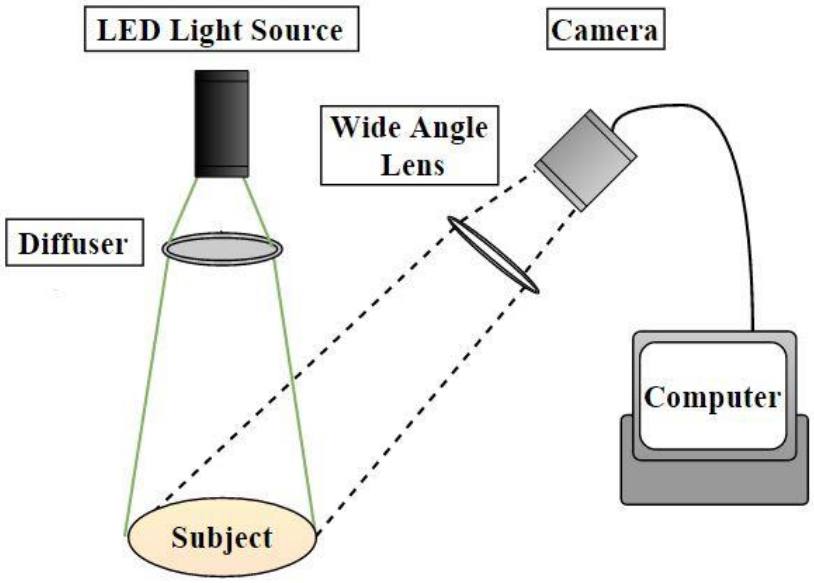

Figure 3. Schematic diagram describing the NIR imaging system

A 0.25x wide angle lens was placed in front of a standard 55 mm photographic lens to produce an image containing each subject's entire forearm.

3.2.2 Testing Performance of NIR Light Source

In order to determine if an optical wavelength is capable of producing higher contrast images of the veins the following test was devised. Images were captured of each subject's forearm using the setup described in Figure 3 at each of the five peak wavelengths described in Section 3.2.1. Histogram equalisation [32] was performed to increase the contrast and ensure that the full dynamic range of image values were used. A high pass two dimensional Butterworth filter was designed in Matlab. It was applied to the image to extract the high frequency components which were amplified and superimposed back onto the original image. This had the effect of sharpening the fine detail within the frame but had a tendency to amplify salt and pepper noise.

Additionally, a median filter was applied to the image, it was effective at smoothing noise within the image but preserved the edge details important for visualisation.

Five images were captured from each subject. It was impossible to make subjects stay exactly still, so image registration [33] was performed to exactly align each image captured at each of the wavelengths. Common points were extracted for each subject corresponding to the skin and the veins. The points were averaged and a ratio of the average intensity between the blood vessels and skin was extracted to provide a metric of comparison between the images captured at different points on the NIR spectrum. The intensity ratio is given by

$$\frac{I_{vein} - I_{skin}}{2^n} \quad (1)$$

where I_{vein} and I_{skin} are the intensities measured from the vein and skin regions and n refers to the number of bits in the image.

3.3 Laser Speckle Imaging System

The following section describes the system developed to perform LSI and how the capabilities of the system were demonstrated.

3.3.1 Development of the LSI System

To perform LSI, a number of additional components were required which are detailed below. Two interchangeable lasers were incorporated into the system design; emitting light at 650 nm or 850 nm respectively. The laser light is passed through a microscopic lens to spread out the beam and a pin-hole lens to filter out higher frequency

components. Finally, the generated light is passed through a diffuser to produce an evenly illuminated interference pattern on a subject. A macro lens was placed in front of the 55 mm photographic lens to increase the level of magnification. To image the speckle field and detect statistical variations relating to blood flow a number of optical requirements must be met. The speckle size, S, must be known in order to properly sample and obtain a representative contrast image [34]. The speckle size, S, was taken to be

$$S = (1.22)(\lambda)(f_{\#})(M) \tag{2}$$

where λ is the wavelength of the laser light source, M is the total magnification of the camera and $f_{\#}$ represents the focal number of the camera lens [35]. The lens $f_{\#}$ was set to 3.2 with a total magnification, M, of 3 times. The speckle size of the 650 nm and 850 nm laser were found to be 7.612 μm and 9.9552 μm. The camera pixel size, as shown in Table 1, is equal to 7.4 μm. Therefore, each speckle is 1.02 pixels and 1.34 pixels using the 650 nm and the 850 nm laser respectively. The spatial sample size in calculations to determine the speckle contrast have to be at least twice the number of pixels in order to satisfy the Nyquist criterion.

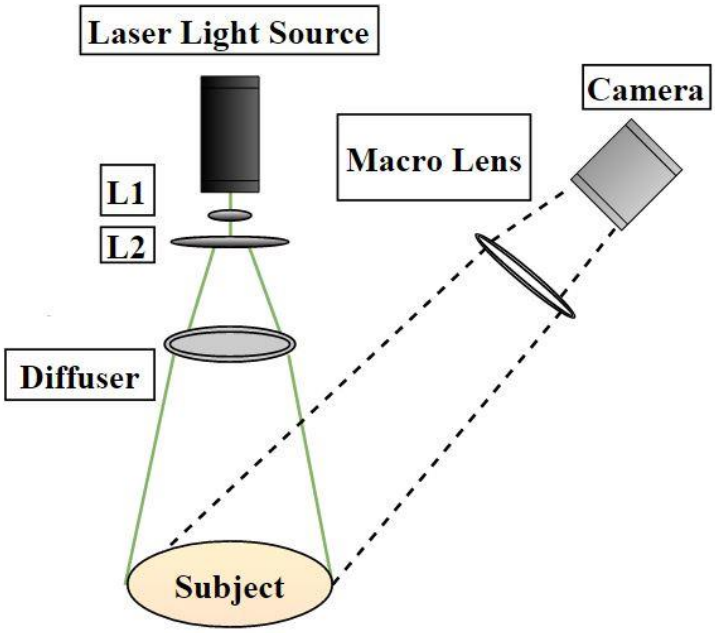

Figure 4. Schematic of laser speckle imaging system

The final LSI imaging system is shown in Figure 4. The laser must be positioned perpendicular to the subject sample to provide even illumination and prevent shadows from distorting the results.

3.3.2 Demonstrating the Ability of LSI to Detect Regions of Blood Flow

LSI was beyond the initial scope of the project. It was implemented with the intention that it could be integrated more fully into the vein visualisation system in future research projects and would provide a base from which more thorough research could be conducted. Two wavelengths of laser light were examined in order to detect blood flow using laser light; 850 nm and 650 nm. The hardware set up is described in Section 3.3.1. Only one subject was used in this test to demonstrate the system's ability to detect blood flow. An area around a vein, identified using the NIR imaging system was illuminated with a speckle interference pattern. Each image was divided into sub-regions and the speckle contrast of each was calculated and used to create a statistical

map differentiating regions of dynamic change, corresponding to blood flow and static unchanging components.

3.4 Eulerian Video Magnification

No additional components were required in order to implement EVM. It was important to determine the accuracy of the technique while extracting a simple diagnostic signal. It was also important to determine how the heart rate signal would be effected by the wavelength of the primary light source. This would indicate if EVM was suitable to be deployed within a NIR vein visualisation system.

In order to compare the extracted heart rate signal to an actual representation of heart rate an external sensor was attached to each subject's finger. The sensor, which uses plethysmography to detect each heart-beat, was not expected to be highly accurate but was deemed to be sufficient to provide a baseline signal with which the estimated signal could be compared. The sensor was connected to an Arduino which was programmed to flash an LED with every pulse. The LED indicator was placed within the frame of each test video so that an actual heart beat signal could be extracted in sync with the estimated heart beat signal from the same video. The system is illustrated in Figure 5 and indicates the addition of the external heart rate indicator.

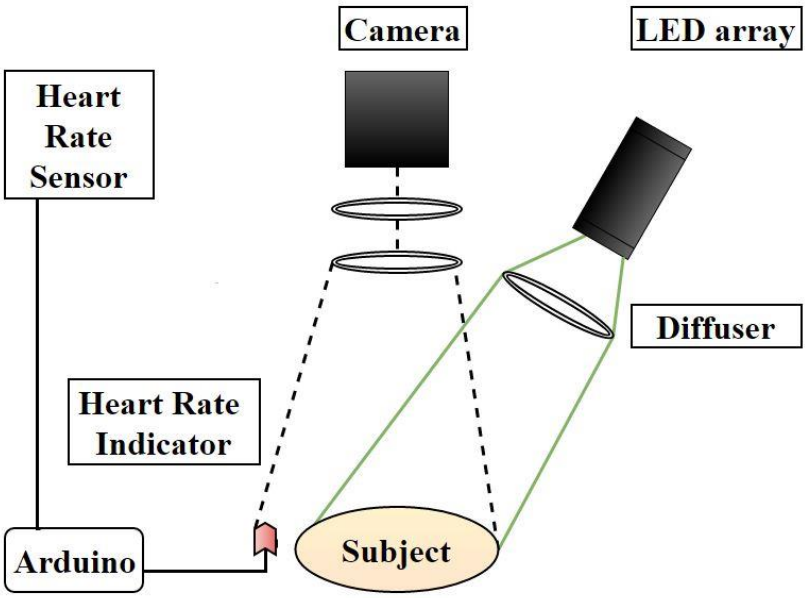

Figure 5. Schematic of system to test the accuracy of EVM

3.4.1 Testing the Accuracy of Heart Rate Extraction using EVM

A section of each subject's forearm was recorded for a duration of ten seconds using five different peak wavelengths; 650 nm, 830 nm, 850 nm and 890 nm. The video was recorded at 20 fps throughout testing, a sampling rate chosen to exceed double the maximum expected frequency within the video and meet the Nyquist criterion. The only light source within the test environment was chosen to operate at DC, ensuring the highest observable frequency would be from the signal of interest which in this case corresponds to heart rate.

Once each video was captured it was processed using the algorithm demonstrated by Wu *et al* [9]. The steps of this video processing method are outlined in Figure 6. A 20 x 20 box was placed on the subject's skin and on the LED indicator representing actual heart rate. The mean squared value of each of the boxes was calculated over

the course of the video and a Matlab function was used to detect the number of peaks within each signal, representing the heart beats. The signals were also visualised to ensure that the peak detection function was working correctly.

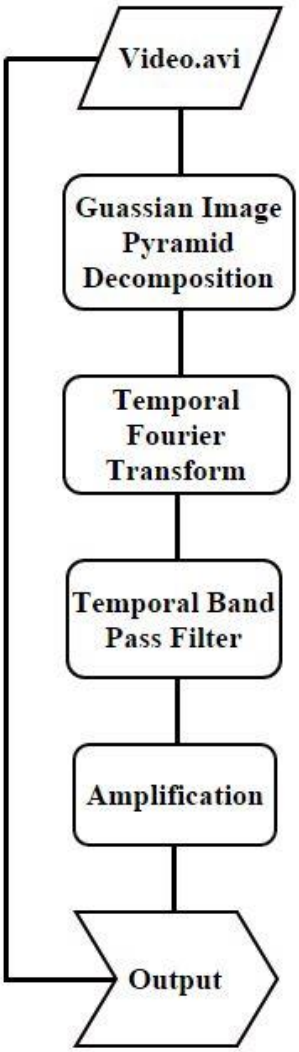

Figure 6. Flow diagram of EVM as proposed by Wu *et al*.

4. Results

Five subjects were asked to participate in each of the three tests. The collected data was anonymised and stored on an encrypted hard drive. A thorough verification of the hardware was performed before each step to ensure correct function. The system test procedures are included within the appendix.

4.1 EVM Heart Rate Extraction Results

Five ten second videos were captured from each of the test subjects at each of the five wavelengths mentioned in Section 3. The signals representing actual and estimated heart rate were compared to develop an understanding of the systems accuracy. Figure 7 shows a representation of the signals which were extracted from the video. The actual heart rate signal lags slightly behind the estimated heart beat signal. This is because blood reaches the point used to estimate the heart rate signal before it reaches the finger tips where the actual heart rate sensor is placed.

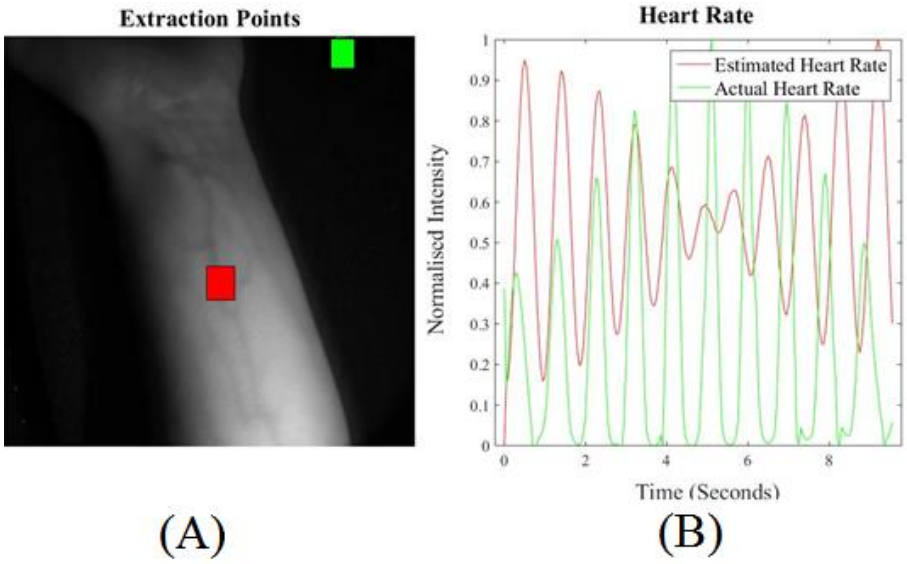

Figure 7. (A). Coloured regions representing the points of signal extraction. In green, the heart rate indicator and red, a flat region of skin (B). The signals extracted from each region

It was found that there was an increase in estimation accuracy when the primary light source lay within the NIR spectrum. In particular, the lowest average error, 3.49%, was recorded while using an 850 nm light source. Comparing this to an average error of 15.6% when a visible 650 nm light source is used, there is an indication that applying EVM within the NIR spectrum yields improvements in signal accuracy.

Table 2 shows the percentage error between the heart rate signals extracted using EVM and the control signal. The maximum estimation error between all the groups appears to be higher in the 650 nm and the 950 nm wavelength than in any of the other groups. Repeatedly the 850 nm wavelength produced the most accurate estimations of heart rate with a negligible error being recorded in three of the five subjects.

Percentage (%) Error Heart Rate Detection By Wavelength					
Subject	650 nm	830 nm	850 nm	890 nm	950 nm
1	25	9.09	0	16.67	23.01
2	16.67	8.34	0	8.34	18.18
3	6.67	20	0	13.34	14.29
4	8.34	15.39	9.09	7.69	16.67
5	21.43	12.56	8.34	14.29	7.69
Mean	15.62	12.56	3.48	11.50	15.98

Table 2. Percentage error of heart rate signal extracted using EVM in comparison to the control signal

The average error between all subjects for each wavelength is shown in Figure 8. The 950 nm wavelength light source interestingly produces a larger error in the extracted heart rate signal when compared to the visible 650 nm wavelength.

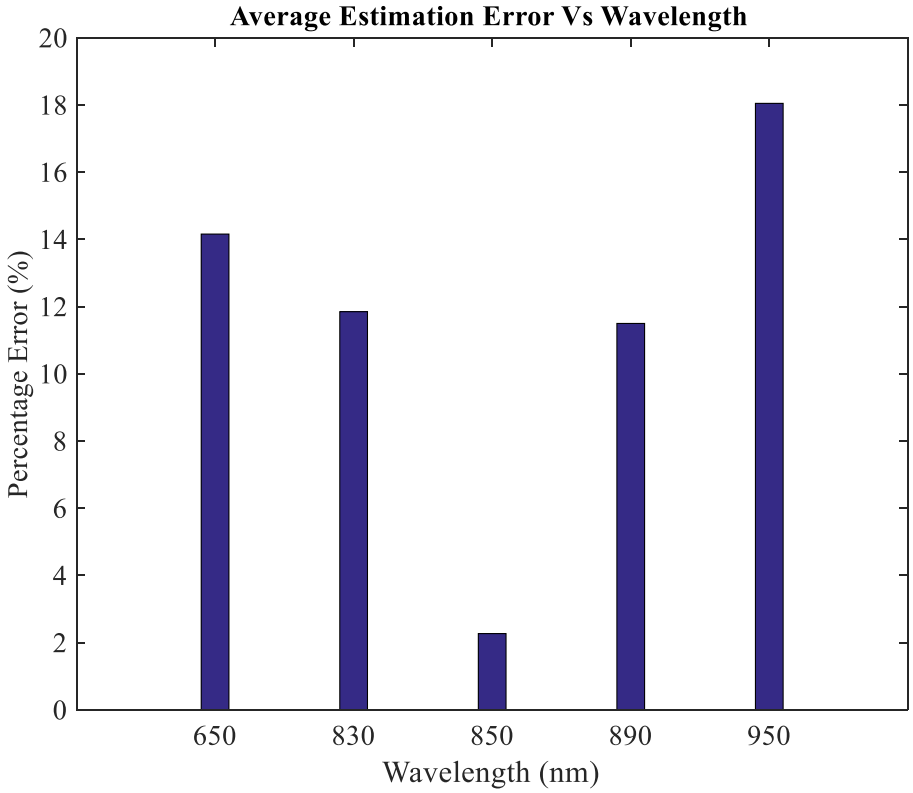

Figure 8. Average error in heart rate detection at each wavelength of light

There is an indication in the results that there is a window within the NIR spectrum capable of allowing higher accuracy signals to be extracted.

4.2 Optimising the Contrast of NIR Images

The same five test subjects were used to test if the wavelength of the NIR light had an effect on the contrast seen between the veins and surrounding tissue. The contrast ratio used to measure the difference between images captured at different wavelengths, was, in every case extracted after enhancing each image using image processing techniques.

The contrast ratio typically followed the same trend between subjects, with the highest average contrast ratio found using the 850 nm light source. While the contrast ratio

tended to decrease in the NIR wavelengths for each subject the actual effectiveness of the technology was quite variable. Between subjects, the number of veins visible was variable, even in subjects with similar skin colours. Table 3 shows the effect of wavelength on the imaged contrast between the veins and surrounding tissue on each subject. The optimal value is one, representing vein and skin points at the maximum and minimum possible intensity values. There is a clear decrease in the average contrast ratio using visible 650 nm light compared to the NIR range of wavelengths. The 850 nm wavelength shows the highest average contrast ratio obtained from images. The 950 nm wavelength consistently produced the lowest contrast ratios of all the NIR wavelengths.

Contrast Ratio As a Function of Wavelength for Each Subject					
Subject	650 nm	830 nm	850 nm	890 nm	950 nm
1	.0541	.3177	.2173	.1655	.3247
2	.1019	.1294	.1655	.1129	.1079
3	.0549	.2070	.1709	.2235	.0486
4	.0962	.2267	.3890	.1827	.0973
5	.1043	.3003	.3608	.1835	.0878
Mean	0.0823	0.2362	.2607	.1736	.1333

Table 3. The average contrast ratio between the blood vessels and the skin of each subject for each wavelength

Figure 9 shows the distribution of the average contrast ratios extracted from each of the five wavelengths and indicates a typical improvement in the contrast ratio values at the 850 nm wavelength.

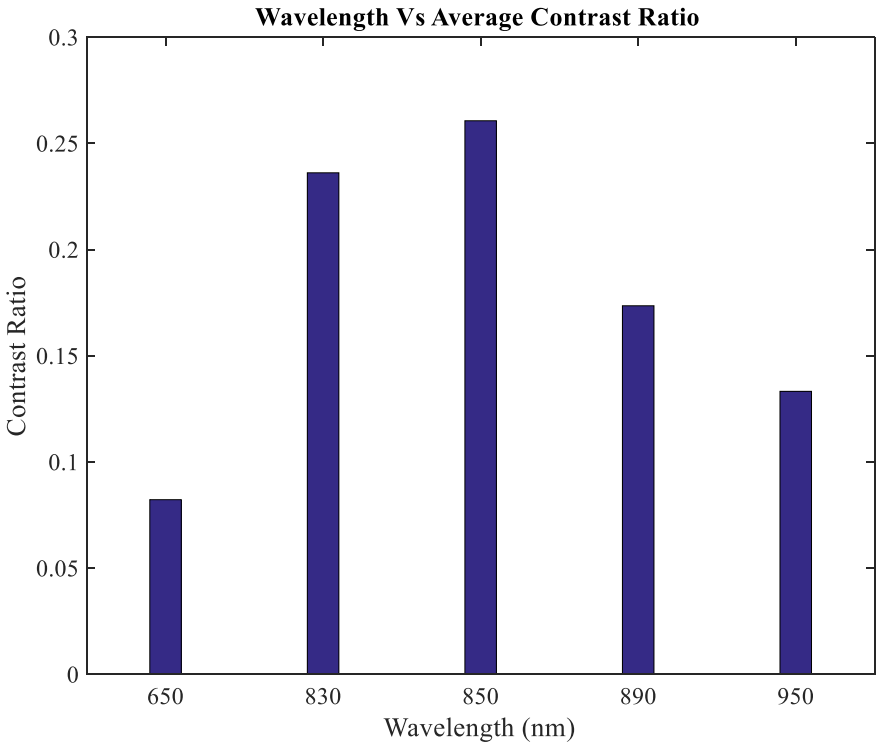

Figure 9. Average contrast ratio between all subjects obtained for each wavelength

To demonstrate the technology a full set of images for one test subject is shown in Figure 10. Each image is captured using light sources providing equal illumination.

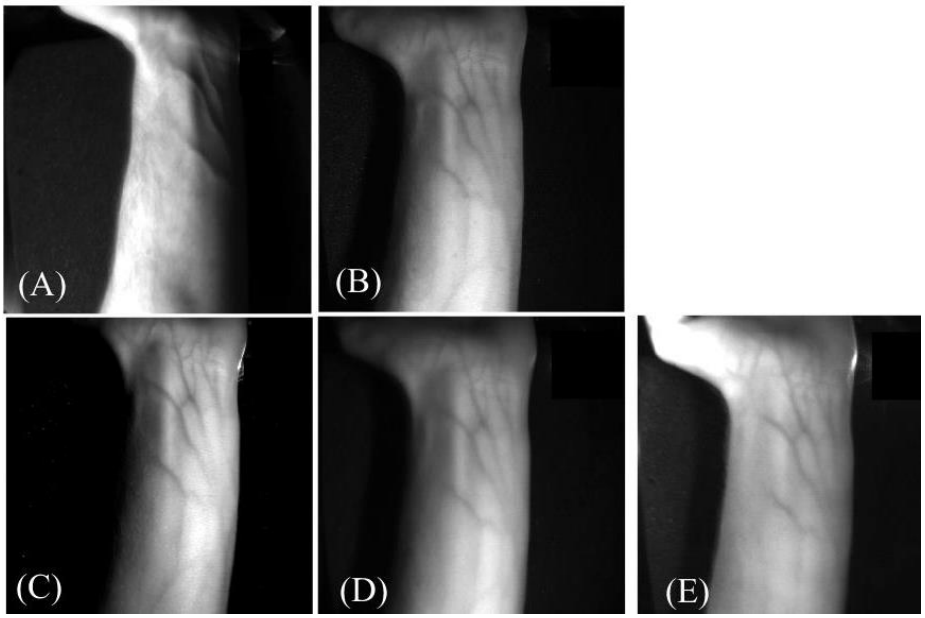

Figure 10. NIR images across wavelength (A). 650 nm (B). 830 nm (C). 850 nm (D). 890 nm (E). 950 nm

The veins match the intensity values of the surrounding skin and are difficult to distinguish clearly. Alternatively, the other NIR images, especially the 850 nm image, show the veins at much lower intensity values than the skin tissue.

4.3 Detecting Blood Flow using LSI

LSI was implemented using two different wavelengths; 650 nm and 850 nm. Laser speckle contrast analysis was implemented to determine if blood flow could be detected. The initial results indicate the potential of the technique and the benefit of applying LSI in the NIR spectrum. On visual inspection, the 850 nm laser light produces images of the veins with as high a contrast as the 850 nm LED light source, indicating the potential to implement both techniques using the same light source and reduce the total number of system components. The NIR vein detection system was used to locate a subcutaneous blood vessel and LSI was used to detect blood flow within. The result pre and post processing is shown in Figure 11.

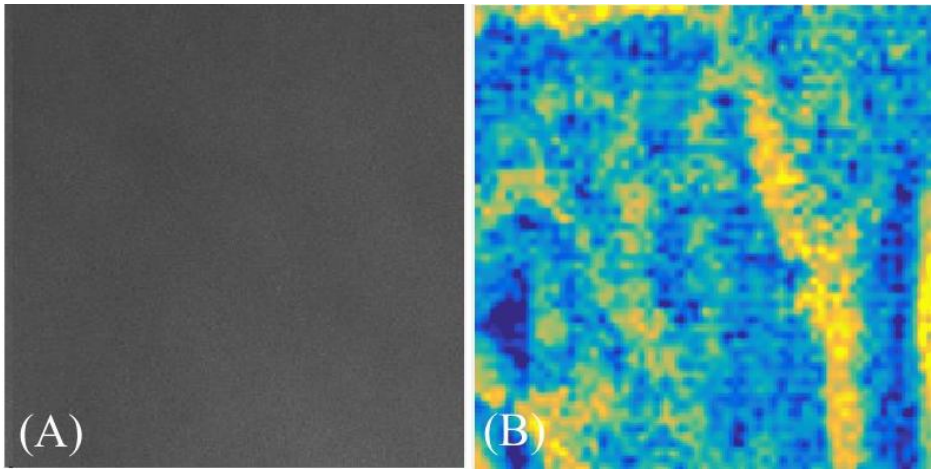

Figure 11. (A) Laser speckle pattern using 850 nm laser (B) Spatial and temporal LSI to highlight blood flow

The same technique was used, using a 650 nm laser light source and the following result is shown in Figure 12. The 850 nm laser light much more clearly defines the veins showing clearer blood flow within the vessels. The 650 nm laser result shows, in yellow, regions of increased movement but does not indicate as precisely where the blood flow is occurring.

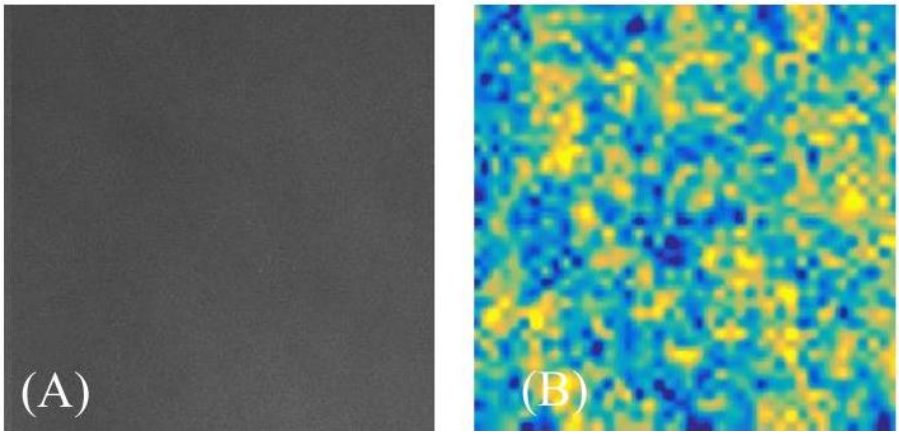

Figure 12. (A) Laser speckle pattern using 650 nm laser (B) Spatial and temporal LSI to highlight blood flow

Figure 12 shows high intensity values representing the dynamic movement of blood in similar positions to the peak intensity points in Figure 11 but the detail is less resolved.

5. Discussion

The following section contains a detailed discussion of the results obtained from each of the three tests. It discusses how the findings compared to similar work within each field and the limitations encountered while implementing each of the three imaging techniques into one system.

5.1 Eulerian Video Magnification

It was shown that heart rate could be extracted remotely using EVM. The technique was implemented using low cost components and did not negatively affect other functions within the vein visualisation system. The error, 15.6% using the visible 650 nm light source was higher than within similar work conducted by Milijkvovic *et al* where heart rate was estimated with an error of less than 5% [36]. The study they conducted only involved two subjects, a possible explanation for the higher reported accuracy.

There is notable variation in the error rates between subjects, suggesting that there are characteristics which alter the effectiveness of the technology. This has been mentioned in other work studying the effect of motion on heart rate signals acquired using EVM [16]. They also noted adverse effects caused by differences in subject skin colour. The use of wavelengths within the NIR spectrum improved the estimation accuracy in every test subject. The 850 nm wavelength, in particular, proved an effective light source at which to visualise veins. In three of the five subjects the signal matched that of the actual heart rate signal and the average error was found to be only 3.48%. The results indicate that within the NIR spectrum certain wavelengths are

more effective at allowing the heart rate signal to be captured using the technique. There are challenges associated with extracting low amplitude signals from videos which are discussed by Guttag *et al* [15]. A possible explanation for the increase in signal accuracy is that the signal, using NIR imaging, is being sampled from a point deeper within the body and as a result of a higher amplitude than when sampled in the visible light spectrum.

Interestingly, the 950 nm wavelength produced a higher average error in comparison to the visible light source. This can be explained by examining the spectral characteristics of both the skin and the camera. Sensitivity of most commercial image sensors is reduced at wavelengths above approximately 900 nm [37]. Lower camera sensitivity would correspond to lower amplitudes of the signal being captured and the introduction of noise into each frame. This could indicate why the error rate increased while estimating the heart rate at this wavelength. Similarly, adipose tissue and water absorb more infrared light above 900 nm than at other points on the NIR spectrum [31] suggesting that this wavelength would produce a signal similar to the one extracted while using a visible light source.

5.2 Near Infrared Imaging

The results of the NIR imaging test showed that the wavelength of light used to visualise the veins played an important role in producing high contrast vein images. The peak wavelength, which produced the highest contrast between the blood vessels and surrounding tissue, was 850 nm. It was shown that in every subject case the contrast ratio increased when the peak wavelength was between 830 nm and 890 nm.

This indicates that a window exists within the NIR spectrum which is capable of highlighting the blood vessels more than the surrounding structures. The 850 nm wavelength light source produced, on average, the highest contrast ratio suggesting that it would be the best light source to use while visualising veins. The findings are similar to those found in other work, where it was suggested that light between 850 nm and 900 nm produced images in which veins could be more easily identified [11].

The results also indicate that the efficacy of the technology is variable between subjects. The skin is optically complex and it is difficult to predict the factors which reduce the performance of the technology. In one study it was suggested that darker skin colour tended to reduce the contrast of the output images [38]. In this work, however, the number of subjects examined was relatively low and no priority was given to subjects with a particular skin colour making it difficult to comment on the effect that darker skin colour has on the technology. Despite the fact that all subjects had a similar skin colour and body fat index there was variability in the results. This indicates that even imperceptible differences in skin colour can alter the efficacy of the technology.

This highlights the importance of incorporating an element of flexibility within the final vein visualisation device. Allowing the user to alter the peak wavelength, adjust the contrast and sharpen the image to produce the best results for the particular patient has been suggested in order to overcome the issue to some extent [12].

5.3 Laser Speckle Imaging

LSI was the least developed element implemented within this project. Early results indicate that the technique is capable of detecting blood flow. Visual inspection of the contrast images show that processing laser speckle patterns both temporally and spatially using established algorithms [24] can produce an impression of blood flow underneath the skin. The speckle pattern produced by the 850 nm laser was able to more clearly visualise blood flow when compared to the 650 nm laser light. Low cost components were used within the design to show that low cost equipment could be used to implement the technique, as shown previously by Richards *et al* [35]. No quantitative measure of blood flow could be determined from the results but analysis of the contrast images showed that regions containing blood vessels were represented by higher values compared to static regions.

Other work expanding on LSI has been demonstrated to be capable of obtaining more quantitative diagnostic information than shown within this project [8][25]. The difference is, however, that the laser light used to produce the speckle pattern was shown to produce a more sensitive determination of blood flow when restricted to a peak wavelength of 850 nm, within the NIR spectrum. The visible laser light showed high intensity values, representing dynamic movement in regions corresponding to the blood vessels, but the region of these higher values was less well defined and not as tightly restricted to areas around the blood vessels.

The algorithm exploiting temporal variations in the speckle field produced a much more highly resolved image but the processing time to produce output was increased. Conversely, the algorithm exploiting the spatial variations in the speckle field

produced output more quickly, but reduced the resolution of the output. The final algorithm used to produce the results shown in this paper involved averaging the spatial variations in the speckle field over a number of frames to achieve a balance between processing time and clarity of results.

5.4 Limitations

Testing was performed on a small population of test subjects to demonstrate each of the three technologies implemented within the proposed vein visualisation system. A larger sample population would have helped to statistically verify the findings of this work. Similarly, access to test subjects with qualities typically suggested to reduce the effectiveness of NIR imaging would have been useful to develop the device to work on a wider range of the population.

The test methods used to quantify and assess system performance were useful in assessing intra-patient variation as a result of different light sources. To better compare results between patients it would have been useful to use another verified imaging modality with which to validate the results. Ultrasound, for example, could have been used to measure blood vessel size, depth and location providing quantitative information to compare with the output of the vein visualisation system. Similarly, specialised ultrasound devices can be used to detect rates of blood flow within the body. This equipment could have been used to determine if a relationship between the statistical properties of the laser speckle interference pattern and the rate of blood flow within the blood vessels could be extracted.

5.5 System Cost

The system was built primarily as a testing device, with interchangeable components implemented into the system design. This allowed flexibility over a range of parameters but did not strictly speaking achieve the original aim of creating one self-contained low cost vein visualisation device. The overall system cost could have been reduced if flexibility of device parameters had been sacrificed. The higher frame rate camera was more expensive than other low fps alternative devices on the market. There would be no adverse effect as a result of using a low-cost image sensor in the proposed system for the reason that the higher frame rate feature was ultimately not required. Similarly, it was found that there was no difference between the laser and LED light sources. The laser could, therefore, be used as the primary light source in both the LSI and NIR applications cutting down on the number of overall system components and cost. While cost may not be as much of a consideration for large clinics, in which vein visualisation devices costing as much as £2,900 [4] are already in use, it is to other consumers. The technology could be useful to individuals if a low cost, reliable solution could be provided. For example, some clinics have allowed long-term patients undergoing kidney dialysis the ability to undergo treatment from home [39]. In most of these cases, increased rates of infection caused this practice to be halted. Vein visualisation technology, cheap enough to be given to each patient, could hold the key to compensating for phlebotomist's experience and reduce infection rates caused by inexperienced vein access [40].

5.6 Future Work

This project has set a foundation on which future work can develop. The device was built with the intention that all components would be interchangeable to determine the variables which effected system performance. With regards to the vein visualisation aspect of the project, two areas show potential for further development. The NIR imaging tests highlighted subject variability as an issue. Testing the technology on a larger population and studying the effects of skin colour on system performance is essential, if widespread clinical implementation is to be possible. Mathematical modelling of the interaction between the complex layers of skin and NIR light could allow algorithms to be implemented. These could compensate for the variability between subjects and hence overcome some of the artefacts interfering with system performance.

Functionality was incorporated into the system to demonstrate LSI. Determining blood flow from the identified blood vessels would represent a step forward and increase the potential use for the technology beyond simple vein access and identification procedures. The test device could be used to develop new ways of extracting more diagnostic information and a range of possible applications, unexplored because of time limitations in this project, could be developed.

EVM was used successfully within this project within a controlled environment. Isolating the light source to the NIR spectrum mitigates the effects of dynamic lighting conditions, representing a step towards clinical implementation. It will be important to develop a way to reduce the effect of motion within video frames. Testing EVM

on moving subjects and developing methods to overcome these effects would make the simple video processing technique far more valuable and robust.

6. Conclusions

A system capable of visualising subcutaneous blood vessels and extracting important diagnostic information was presented. NIR imaging techniques were used to develop a simple vein visualisation system capable of highlighting otherwise imperceptible blood vessels. A measure of the system's ability to distinguish blood vessels was developed and allowed an in depth examination of the effect of the primary light source on the effectiveness of the technology. An 850 nm peak wavelength produced the highest contrast between the blood vessels and surrounding tissue, indicating a window within the NIR spectrum at which vein visualisation performance is maximised.

The utility of the vein visualisation system presented was increased by implementing two additional techniques into the system. EVM was demonstrated to show that heart rate could be extracted remotely. It was shown that the error of the estimated heart rate signal could be reduced by restricting the primary light source to the NIR spectrum. Similarly, system tests on the heart rate monitoring component of the device showed that the accuracy was maximised when the primary light source had a peak wavelength of 850 nm.

Finally, LSI was incorporated into the device to determine more quantitative diagnostic information about blood flow within the imaged veins. The technique was demonstrated to be capable of highlighting regions of blood flow. It was also shown that laser light of 850 nm was better able to isolate regions of blood flow compared to visible, 650 nm, laser light. No quantitative measurements could be extracted but a

framework was set up for future research to develop the concept integrated into the system.

The work also highlighted that vein visualisation technology is variable throughout subject groups. In every subject, veins were detected at a higher contrast but the overall number of additional blood vessels that could be visualised varied dramatically between subjects. Heart rate detection using EVM showed less variability but did present a number of limitations which could hinder the technology in a real world clinical setting. The results were highly sensitive to uncontrolled movement and lighting within video frames which could present problems in clinical settings.

In conclusion a system was developed capable of visualising blood vessels underneath the skin. Established technologies were combined to produce one device which is more capable than other established vein visualisation devices.

7. References

[1] K. Konner, “A primer on the av fistula - Achilles’ heel, but also Cinderella of haemodialysis,” *Nephrol. Dial. Transplant.*, **vol. 14**, pp. 2094–2098, (1999).

[2] K. Taxbro, S. Berg, F. Hammarskjöld, H. Hanberger, and B.-E. Malmvall, “A prospective observational study on 249 subcutaneous central vein access ports in a Swedish county hospital.,” *Acta Oncol.*, **vol. 52**, pp. 893–901, (2013).

[3] R. N. Kaddoum, D. L. Anghelescu, M. E. Parish, B. B. Wright, L. Trujillo, J. Wu, Y. Wu, and L. L. Burgoyne, “A randomized controlled trial comparing the AccuVein AV300 device to standard insertion technique for intravenous cannulation of anesthetized children,” *Paediatr. Anaesth.*, **vol. 22**, pp. 884–889, (2012).

[4] NHSC, “AccuVein ® AV300 peripheral vein imaging device,” National Institute for Health Research, University of Birmingham, United Kingdom, pp. 1–2, (2010).

[5] A. Matas, M. G. Sowa, G. Taylor, and H. H. Mantsch, “Melanin as a confounding factor in near infrared spectroscopy of skin,” *Vib. Spectrosc.*, **vol. 28**, pp. 45–52, (2002).

[6] J. M. Fields, A. J. Dean, R. W. Todman, A. K. Au, K. L. Anderson, B. S. Ku, J. M. Pines, and N. L. Panebianco, “The effect of vessel depth, diameter, and location on ultrasound-guided peripheral intravenous catheter longevity,” *Am. J. Emerg. Med.*, **vol. 30**, pp. 1134–1140, (2012).

[7] Y. Bishitz, N. Ozana, Y. Beiderman, F. Tenner, M. Schmidt, V. Mico, J. Garcia, and Z. Zalevsky, “Noncontact optical sensor for bone fracture diagnostics,” *Biomed. Opt. Express*, **vol. 6**, p. 651-657, (2015).

[8] P. Zakharov, A.C. Völker, M. T. Wyss, F. Haiss, N. Calcinaghi, C. Zunzunegui, A. Buck, F. Scheffold, and B. Weber, “Dynamic laser speckle imaging of cerebral blood flow.,” *Opt. Express*, **vol. 17**, pp. 13904–13917, (2009).

[9] H.-Y. Wu, M. Rubinstein, E. Shih, J. Guttag, F. Durand, and W. Freeman, “Eulerian video magnification for revealing subtle changes in the world,” *ACM Trans. Graph.*, **vol. 31**, pp. 1–8, (2012).

[10] F. B. Chiao, F. Resta-Flarer, J. Lesser, J. Ng, A. Ganz, D. Pino-Luey, H. Bennett, C. Perkins, B. Witek, and H. C. Hemmings, “Vein visualization: Patient characteristic factors and efficacy of a new infrared vein finder technology,” *Br. J. Anaesth.*, **vol. 110**, pp. 966–971, (2013).

[11] N. J. Cuper, J. H. G. Klaessens, J. E. N. Jaspers, R. de Roode, H. J. Noordmans, J. C. de Graaff, and R. M. Verdaasdonk, “The use of near-infrared light for safe and effective visualization of subsurface blood vessels to facilitate blood withdrawal in children,” *Med. Eng. Phys.*, **vol. 35**, pp. 433–440, (2013).

[12] S. Juric and B. Zalik, “An innovative approach to near-infrared spectroscopy

using a standard mobile device and its clinical application in the real-time visualization of peripheral veins," *BMC Med. Inform. Decis. Mak.*, **vol. 14**, p. 1- 9, (2014).

[13] H. Akbari, Y. Kosugi, K. Kojima, and N. Tanaka, "Blood vessel detection and artery-vein differentiation using hyperspectral imaging.," *31st Annu. Int. Conf. IEEE Eng. Med. Biol. Soc.*, pp. 1461–1464, (2009).

[14] S. Gläser, N. Friedrich, B. Koch, C. Schäper, H. Völzke, S. B. Felix, K. Empen, A. Hannemann, R. Ewert, and M. Dörr, "Exercise blood pressure and heart rate reference values," *Hear. Lung Circ.*, **vol. 22**, pp. 661–667, (2013).

[15] A. Zhao and J. Guttag, "Estimating a Small Signal in the Presence of Large Noise," *2015 IEEE International Conference on Computer Vision Workshop*, pp. 671-676, (2015).

[16] A. Alzahrani and A. Whitehead, "Preprocessing Realistic Video for Contactless Heart Rate Monitoring Using Video Magnification," *Proc. -2015 12th Conf. Comput. Robot Vision, CRV 2015*, pp. 261–268, (2015).

[17] C. Liu, H. Gomez, M. R. Pinsky, B. Zuckerbraun, and A. Dubrawski, "Real-time Visual Analysis of Microvascular Blood Flow for Critical Care," *2015 IEEE Conference on Computer Vision and Pattern Recognition (CVPR)*, Boston, MA, pp. 2217-2225, *(2015)*.

[18] L. Lévesque, "Nyquist sampling theorem : understanding the illusion of a spinning wheel captured with a video camera,", *Physics Education*, **vol. 49**, pp. 697 -705, (2014).

[19] V. Jeanne, M. Asselman, B. Den Brinker, and M. Bulut, "Camera-based heart rate monitoring in highly dynamic light conditions," *2013 International Conference on Connected Vehicles and Expo (ICCVE)*, pp. 798–799, (2013).

[20] A. Shahzad, N. M. Saad, N. Walter, A. S. Malik, and F. Meriaudeau, "An efficient method for subcutaneous veins localization using Near Infrared imaging," *2014 5th Int. Conf. Intell. Adv. Syst.*, pp. 1–4, (2014).

[21] Y. Rakhshani Fatmehsari and Z. Moussavi, "Designing and Implementing a Portable Near-Infrared Imaging System for Monitoring of Human's Functional Brain Activity," *J. Med. Device.*, **vol. 9**, pp. 1-2, (2015).

[22] M. Francon and H. Arsenault, "Speckle in the image of an object illuminated by laser light," in *Laser speckle and applications in optics*, 1st ed. Paris, France, Academic Press, pp. 1-19, (1979).

[23] J. D. Briers and S. Webster, "Laser speckle contrast analysis (LASCA): a nonscanning, full-field technique for monitoring capillary blood flow," *J. Biomed. Opt.*, **vol. 1**, pp. 174–179, (1996).

[24] M. Z. Ansari and A. K. Nirala, "Monitoring capillary blood flow using laser speckle contrast analysis with spatial and temporal statistics," *Opt. - Int. J. Light Electron Opt.*, **vol. 126**, pp. 5224–5229, (2015).

[25] N. Yokoi and Y. Aizu, "Probing depth and dynamic response of speckles in

near infrared region for spectroscopic blood flow imaging," *Opt. Laser Technol.*, **vol. 78**, pp. 106–114, (2016).

[26] O. Yang and B. Choi, "Laser speckle imaging using a consumer-grade color camera.," *Opt. Lett.*, **vol. 37**, pp. 3957–3959, (2012).

[27] Y. Shimada, T. Okumura, T. Nagata, S. Sawada, K. Matsui, R. Hori, I. Yoshioka, T. Yoshida, R. Osada, and K. Tsukada, "Usefulness of blood supply visualization by indocyanine green fluorescence for reconstruction during esophagectomy," *Esophagus*, **vol. 8**, pp. 259–266, (2011).

[28] Y. Mitani, A. Kubota, M. Ueno, K. Takifuji, T. Watanabe, S. Hayami, S. Kounami, H. Tsujimoto, and H. Yamaue, "Real-time identification of hepatoblastoma using a near infrared imaging with indocyanine green," *J. Pediatr. Surg. Case Reports*, **vol. 2**, pp. 180–183, (2014).

[29] H. D. Reidenbach, "The Laser Safety Officer - Current and future regulations in Germany," *Med. Laser Appl.*, **vol. 25**, pp. 75–83, (2010).

[30] Anonymous, "Z136 ASC : An Update on Laser Safety Standards," *Professional Safety*,**vol. 53**, pp. 27, (2008).

[31] C.-H. Quek and K. W. Leong, "Near-Infrared Fluorescent Nanoprobes for in Vivo Optical Imaging," *Nanomaterials*, **vol. 2**, pp. 92–112, (2012).

[32] A. M. Reza, "Realization of the contrast limited adaptive histogram equalization (CLAHE) for real-time image enhancement," *J. VLSI Signal Process. Syst. Signal Image. Video Technol.*, **vol. 38**, pp. 35–44, (2004).

[33] T. D. Linh and H. Q. Linh, "Medical image registration in matlab," *Department of Biomedical Engineering-Faculty of Applied Science*, HCMC University of Technology, Vietnam.

[34] S. J. Kirkpatrick, D. D. Duncan, and E. M. Wells-Gray, "Detrimental effects of speckle-pixel size matching in laser speckle contrast imaging.," *Opt. Lett.*, **vol. 33**, pp. 2886–2888, (2008).

[35] L. M. Richards, S. M. S. Kazmi, J. L. Davis, K. E. Olin, and A. K. Dunn, "Low-cost laser speckle contrast imaging of blood flow using a webcam.," *Biomed. Opt. Express*, **vol. 4**, pp. 2269–83, (2013).

[36] N. Miljkovie and D. Trifunovie, "Pulse rate assessment: Eulerian Video Magnification vs. electrocardiography recordings," *12th Symp. Neural Netw. Appl. Electr. Eng. NEUREL 2014 - Proc.*, pp. 17–20, (2015).

[37] E. Berra, S. Gibson-Poole, A. MacArthur, R. Gaulton, and A. Hamilton, "Estimation of the Spectral Sensitivity Functions of Un-Modified and Modified Commercial Off-the-Shelf Digital Cameras To Enable Their Use As a Multispectral Imaging System for Uavs," *ISPRS - Int. Arch. Photogramm. Remote Sens. Spat. Inf. Sci.*, **vol. 1**, pp. 207–214, (2015).

[38] O. Van Der Woude, N. J. Cuper, C. Getrouw, C. J. Kalkman, and J. C. De Graaff, "The effectiveness of a near-infrared vascular imaging device to support intravenous cannulation in children with dark skin color: A cluster

randomized clinical trial," *Anesth. Analg.*, **vol. 116**, pp. 1266–1271, (2013).

[39] I. Ledebo, "What limits the expansion of self-care dialysis at home," *Hemodial. Int.*, **vol. 12**, , pp. 55–60, (2008).

[40] B. J. Manns, K. Taub, C. VanderStraeten, H. Jones, C. Mills, M. Visser, and K. McLaughlin, "The impact of education on chronic kidney disease patients' plans to initiate dialysis with self-care dialysis: A randomized trial," *Kidney Int.*, **vol. 68**, pp. 1777–1783, (2005).

Appendix I

Matlab Code

Eulerian Video Magnification Code

```
%Sets up output directory to store result
working_directory = './output';
resultsDir = 'output';

%Names Resulting Output with parameters contained within output name
Output_Video = fullfile(working_directory,[vid_name '-' num2str(freq_low)'hz-to-'
num2str(freq_high)'hz -alpha-' num2str(amplification)'.avi']);

%Extract input video parameters
Video       =  VideoReader(vid_name);   %Video Name
Height      =  Video.Height;            %Video Pixel Height
Width       =  Video.Width;             %Video Pixel Width
fps         =  Video.FrameRate;         %Video Frame Rate
nChannels   =  3;                       %Specify Number of Video Channels
length      =  Video.NumberOfFrames;    %Number of Frames in Video

%Initialise Temporary storage Structure for output
temp = struct('cdata', zeros(Height , Height , nChannels, 'uint8'), 'colormap', []);

startIndex = 1;                         %initialise start index
endIndex = length-10;                   %video terminates before the end of the video

vidOut = VideoWriter(Output_Video);     %Creates a video object to store output video
vidOut.FrameRate = fps;                 %Output Playback Speed
open(vidOut)                            %Open Video object for writing

rgbframe = read(Video, startIndex);   %Read the first frame of the input video
frame = im2double(rgbframe);            %convert indexed image values to double

gaussPyramid = vision.Pyramid('PyramidLevel',4) ; %Gaussian Image Pyramid -
Decomposition and Downsampling
blurred = step(gaussPyramid,frame);               %Apply Image Pyramid Operation to
first video frame

GDown_stack = zeros(endIndex - startIndex +1,
size(blurred,1),size(blurred,2),size(blurred,3)); %Create a memory structure
containing space for all downsampled images
GDown_stack(1,:,:,:) = blurred;                   %Fill first compartment with first
Gaussian Pyramid Frame

 k = 1;                                           %Specify first position in array
 for i=startIndex+1:endIndex                      %First frame filled, iterate
through frame 2 to the last frame
```

```
            k = k+1;
            rgbframe = read(Video, i);          %Read in each frame
            frame = im2double(rgbframe);        %Convert and store as a double
            blurred = step(gaussPyramid,frame); %Reduce Gaussian Pyramid
            GDown_stack(k,:,:,:) = blurred;     %Fill up empty memory structure

 end


 input_shifted = shiftdim(GDown_stack,0);   %Same as squeeze function - removes
singleton dimension
 Dimensions = size(input_shifted);          %size of new downsampled video required
 n = Dimensions(1);
 Dimensions(1) = 1;
 dn = size(Dimensions,2);

 %Create a mask for ideal filter operations
 Freq = 1:n;
 Freq = (Freq-1)/n*sample_rate;
 mask = Freq > freq_low & Freq < freq_high; %Create ideal band pass filter
 mask = mask(:);
 mask = repmat(mask, Dimensions);

 %Transform the video of downsampled frames over the temporal domain.
 F = fft(input_shifted,[],1);   %Transform video , along frames, to frequency domain
 F(~mask) = 0;                  %apply ideal filter to isolate particular temporal
frequencies

 filtered = real(ifft(F,[],1)); %Inverse transform to revert back from temporal
frequency domain
 filtered_stack  = shiftdim(filtered,dn); %recreate Video

redChannel = filtered_stack(:, :, 1);           %fill three channels with result
greenChannel = filtered_stack(:, :, 2);         %not strictly necesscary
blueChannel = filtered_stack(:, :, 3);          %

%Additional binary mask operations
% filtered_stack(:, :, 1) = filtered_stack(:, :, 1) .* amplification ;     %remove
the values occurring at lower intensities
% filtered_stack(:, :, 2) = filtered_stack(:, :, 2) .* amplification ;     %remove
the values occurring at lower intensities
% filtered_stack(:, :, 3) = filtered_stack(:, :, 3) .* amplification ;     %remove
the values occurring at lower intensities
filtered_stack(:,:,:) = filtered_stack(:,:,:) .* amplification;         %amplify the
result linearly

startIndex = 1;                                 %reinitialise the starting index
myavi = VideoWriter(Output_Video);              %create a video object
myavi.FrameRate = 1;                            %Playback frame rate set to 1
open(vidOut);

k = 0;
window1 = 40;           %Size of skin average box
window2 = 40;           %size of reference average box
counter = 1;
beats = 0;
```

```
    for i=startIndex:endIndex    %iterate through every processed frame, adding
original frames to amplified image mask
        k = k+1;
        frame= read(Video, i);    %read in an image frame
        frame = im2double(frame);
        frame = imadjust( frame,[0 0.9],[]);  %Saturate the upper and lower max
values to improve contrast

        filtered = squeeze(filtered_stack(k,:,:,:));        %process each frame of
amplified temporal frequency container
        floor(x_coord1)                                     %GUI functionality
        floor(x_coord2)                                     %GUI functionality
        floor(y_coord1)                                     %GUI functionality
        floor(y_coord2)                                     %GUI functionality
        filtered = imresize(filtered,[Height Width]);

        frame =  filtered+frame;                            %combine amplified mask
and original video

        %Extract average of two regions selected for each frame
        heart_rate_m(i) =
(mean2(frame(floor(y_coord1):floor(y_coord1)+window1,floor(x_coord1):floor(x_coord1+w
indow1))));
        heart_rate_v(i) =
(mean2(frame(floor(y_coord2):floor(y_coord2)+window2,floor(x_coord2):floor(x_coord2+w
indow2))));
        %Square signals for beat extraction
        heart_rate_v(i) = heart_rate_v(i)*heart_rate_v(i) ;
        heart_rate_m(i) = heart_rate_m(i)*heart_rate_m(i) ;


        %Improve Visualisation in GUI
        %Mark selected rectangles by user on the visualisation

frame(floor(y_coord1):floor(y_coord1)+window1,floor(x_coord1):floor(x_coord1+window1)
) = 0;

frame(floor(y_coord2):floor(y_coord2)+window2,floor(x_coord2):floor(x_coord2+window2)
) = 0;

        %Compute time of signal in seconds determined by video frame rate
        l_time = [0:1/sample_rate:i/sample_rate-1/sample_rate];

        imagesc(frame);
        hold all;
        axis off
        %Mark regions of beat signal extraction
        rectangle('Position',[x_coord1 y_coord1 window1 window1],'Curvature',0.2)
        rectangle('Position',[x_coord2 y_coord2 window2 window2],'Curvature',0.2)
        hold off;
        axes(handles.axes2);

        if(i == endIndex)
            figure;subplot(1,2,1)
            imshow(frame)
```

```
            subplot(1,2,2)

        end
        %extract normalised heart rate signal - Average and square
        %specified region - plot live values for visualisation

        plot( l_time,((heart_rate_m-min(heart_rate_m))/(max(heart_rate_m)-
min(heart_rate_m))),'r')
        title('Heart Rate ')
        xlabel('Time (S)')
        ylabel('Normalised Intensity')
        hold all;
        plot( l_time,((heart_rate_v-min(heart_rate_v))/(max(heart_rate_v)-
min(heart_rate_v))),'g')
        legend('Estimated Heart Rate', 'Actual Heart Rate')
        hold off

        axes(handles.axes1);

        writeVideo(vidOut, frame);
        refresh;


    end

    %Power of signal to extract beat characteristics
    x = heart_rate_m.^2;
    y = heart_rate_v.^2;

    axes(handles.axes2);
    hold all

%   PKS = findpeaks(Y) finds local peaks in the data vector Y. A local peak
%   is defined as a data sample which is either larger than the two
%   neighboring samples or is equal to Inf.

  BPM = findpeaks(x,'MinPeakDistance',10 )
  BPM_ref = findpeaks(y,'MinPeakDistance',10)

  x_s = num2str(numel(BPM))             %display estimated bpm
  y_s = num2str(numel(BPM_ref))         %display actual bpm

  handles.text24.String = y_s           %Reference Heart rate peaks
  handles.text26.String = x_s           %Estimated Heart rate Peaks
  close(vidOut);

 clear heart_rate_m, heart_rate_v;
```

NIR Image Enhancement Code

```
%Processes automatically video to increase sharp details and
%stetch the histogram using histogram equalisation
%intended to be used with videos taken in the NIR spectrum in order to
%enhance vein visualisation effectiveness

%Setup Output Video Parameters - INPUT FROM USER GUI
vid_name  =  (get(handles.edit13,'String'))             %Video input name
clip = (str2double(get(handles.edit16,'String')))       %determine extent of contrast
increase
wc = (str2double(get(handles.edit17,'String')))         %determine high pass filter
cut off frequency
Test_Video      =  VideoReader(vid_name);
imagenew = 0;

%Select which image processing operations are performed
checkbox_state = get(handles.checkbox1,'Value') ;       %Turn on Contrast Adjustment
checkbox_state1 = get(handles.checkbox2,'Value') ;      %Turn on Brightness
enhancement
checkbox_state2 = get(handles.checkbox3,'Value') ;      %Turn on High pass filter

t = string(datetime('now','TimeZone','local','Format','d-MMM-y-HH-mm-ssZ'))
%findcurrent time to incorporaate into filename
%initialise video name and object
vid_name =   sprintf( '%s-NIR-%d.avi',vid_name,t);      %Video output is named:
video_output-NIR-{current time}
myavi = VideoWriter(vid_name);
open(myavi);                                            %open described video object
to place output in

lengthv =  Test_Video.Duration;

for i = 1:lengthv

image =   read(Test_Video, i);      %Read in original image
%---Display original image to illustrate effect of enhancements-----------
axes(handles.axes1);
imshow(image)
title('Original')
axis off;
%------------------------------------------------------------------------

%Maximise the image contrast - stretch values between 0 - 255 in 8 bit
%images
if(checkbox_state1 ~= 0)            %Histogram equalisation

%Saturate the top and bottom 1% of values to increase contrast
%image = imadjust(image)
%image = imadjust(image, [.1 .7])

%image = histeq(image) %standard histogram equalisation
```

```
%Best Results - adjusts histogram for sub regions within the image
image = adapthisteq(image,'clipLimit',clip,'Distribution','rayleigh');  %Contrast-
limited adaptive histogram equalization (CLAHE)

end

%Increase the brightness of the image
if(checkbox_state ~= 0)

    h = [2];    %create a 1 x 1 image mask with a sum over 1 to increase the image
brightness
    image = imfilter(image,h);  %Apply brightness filter

end

%Add result of a high pass filters to orgiginal image to increase sharpness
if(checkbox_state2 ~= 0)

b = fir1(10,wc,'high')               %design a high pass 1d filter
%1d filter coefficients
%b = [0.0000   -0.0079   -0.0402   -0.1033   -0.1708    0.8005   -0.1708   -0.1033
-0.0402   -0.0079    0.0000];

h = ftrans2(b);                      %convert 1d filter to two dimensions

%2d filter coefficients
% h =  [0         0         0         0         0         0         0         0
0         0         0;
%       0   -0.0000   -0.0002   -0.0009   -0.0017   -0.0022   -0.0017   -0.0009   -
0.0002   -0.0000         0;
%       0   -0.0002   -0.0016   -0.0048   -0.0084   -0.0101   -0.0084   -0.0048   -
0.0016   -0.0002         0;
%       0   -0.0009   -0.0048   -0.0125   -0.0211   -0.0249   -0.0211   -0.0125   -
0.0048   -0.0009         0;
%       0   -0.0017   -0.0084   -0.0211   -0.0343   -0.0398   -0.0343   -0.0211   -
0.0084   -0.0017         0;
%       0   -0.0022   -0.0101   -0.0249   -0.0398    0.9544   -0.0398   -0.0249   -
0.0101   -0.0022         0;
%       0   -0.0017   -0.0084   -0.0211   -0.0343   -0.0398   -0.0343   -0.0211   -
0.0084   -0.0017         0;
%       0   -0.0009   -0.0048   -0.0125   -0.0211   -0.0249   -0.0211   -0.0125   -
0.0048   -0.0009         0;
%       0   -0.0002   -0.0016   -0.0048   -0.0084   -0.0101   -0.0084   -0.0048   -
0.0016   -0.0002         0;
%       0   -0.0000   -0.0002   -0.0009   -0.0017   -0.0022   -0.0017   -0.0009   -
0.0002   -0.0000         0;
%       0         0         0         0         0         0         0         0
0         0         0;]


image = image + imfilter(image,h);  %Add result ontop of original to make edges
clearer

%non linear filter to remove salt and pepper noise and preserve edges.
image = medfilt2(image);            %spatial filtering median non linear filter
```

```
%Sharpening filter
%h = fspecial('laplacian');
%image =image + imfilter(image,h);

%Sharpening filter
%h = fspecial('prewitt');
%image =image + imfilter(image,h);

%Sharpening filter  - prewitt filter
%h =  [1     1     1;
%      0     0     0;
%     -1    -1    -1;];


%image = image + imfilter(image,h);
end

%Display image in GUI
axes(handles.axes4);
imshow(image)
title('Enhanced')
axis off
hold on;
%create video
set(gca,'nextplot','replacechildren');
currFrame = getframe( handles.axes4 );
writeVideo(myavi, currFrame);

axes(handles.axes1);

end
```

Image Registration Code

```
%Included to highlight basic image registration - applied to project image
%in next section
%Preliminary Image Registration

%load reference image
I =  imread('./image1.jpg');            %Read in reference image
%Load moving iamge
I1 = imread('./image2.jpg');

cpselect(I1,I)                          %opengui to select points common between
original image and new image
movingPointsAdjusted = cpcorr(movingPoints,fixedPoints,I1(:,:,1),I(:,:,1));    %fine
tune selected points - cross correlation

%affine selected - skew, translation, and rotation -
t = cp2tform(movingPointsAdjusted,fixedPoints,'affine' ) ;    %create transform
```

```
structure - similarits min of 3 pairs

registered = imtransform(I1,t, 'XData',[1 length(I(:,1,1))], 'YData',[1
length(I(1,:,1))]);  %apply transform structure to original image and plot result
figure, imshowpair(registered,I)
%original image is rotated to match rotated imag
```

```
%Alternative intensity based registration method
%not as suitable for particular application

I = imread('Visible.bmp');              %Read in one image
I1 = imread('Infrared.bmp');            %Read in image two

[optimizer, metric] = imregconfig('multimodal') %tune the optimisation function to
work better with images from different sensors
                                                %mulitmodal chosen because
                                                %the change in light
                                                %wavelength essentially
                                                %makes the camera act as a
                                                %separate sensor.

optimizer.InitialRadius = 0.009;                %the selected initial radius
determines how quickly solution converges
optimizer.Epsilon = 1.5e-4;                     %epsilon determines how much guess
changes iteratively
optimizer.GrowthFactor = 1.01;
optimizer.MaximumIterations = 300;              %Iterations optimisation function
performs to find best fit - loss function

movingRegistered = imregister(I1, I, 'affine', optimizer, metric);  %affine - perfomr
the intensity based registration
helperVolumeRegistration(I,movingRegistered)
figure;
imshowpair(I, movingRegistered,'Scaling','joint');
```

C++ Code

Implementation of EVM in C++

```
/* Real time implementation of Eulerian Video Magnification

    adaption of work by MIT publication "Eulerian Video Magnification"
    Implemented in OpenCv V 3.00
    Requires Pylon c++ API
    */

Mat cv_img, temp_img;                   //declare reference images
Mat Buffer[WINDOW], Buffer1[WINDOW];    //decalre buffer image, WINDOW is lengt
h of buffer - declares length of time temporal freqs are determined in
Mat image32f_1;                         //Holder float type image
```

```
int counter = 0, counter1 = 0;
try
{

    //Initialise Camera -
    CPylonImageWindow imageWindows[1];                                  //Declare pylon image Window
    Camera_t camera(CTlFactory::GetInstance().CreateFirstDevice());     //Initialise Camera Device
    camera.Open();                                                      //Open Basler Camera Device
    camera.Width = width_c;                                             //Frame Heigth
    camera.Height = height_c;                                           //Frame Width
    camera.ExposureTime = exposure_c;                                   // GUI specified Exposure
    camera.AcquisitionFrameRateEnable = true;                           // Enable user to set frame rate
    camera.AcquisitionFrameRate = 20;                                   //Frame Rate must be limited to 20 - buffer must be over 20 samples (1 second) long
    camera.StartGrabbing(1, GrabStrategy_LatestImageOnly);              //Set up image aquisition
    //camera.SensorReadoutMode = SensorReadoutMode_Fast;                //To enable max frame rates set sensor read out mode to fast

    CGrabResultPtr ptrGrabResult;
    ::Sleep(800);
    do
    {

        yes = iskeypressed();                                           //Check if end preview flag has been set
        camera.RetrieveResult(5000, ptrGrabResult, TimeoutHandling_ThrowException); //Retrieve camera output
        if (ptrGrabResult->GrabSucceeded())
        {
            CPylonImage image;                                      //Pylon image must be converted to openCv Mat
            CImageFormatConverter converter;                        //Declare converter
            converter.OutputPixelFormat = PixelType_BGR8packed; //BGR type conversion
            converter.OutputBitAlignment = OutputBitAlignment_MsbAligned;

            bool windowCreated = false;

            camera.StartGrabbing(1, GrabStrategy_LatestImageOnly);  //Start Grabbing
            converter.Convert(image, ptrGrabResult);                //convert captured image
            cv_img = cv::Mat(ptrGrabResult->GetHeight(), ptrGrabResult->GetWidth(), CV_8UC3, (uint8_t*)image.GetBuffer()); // create opencv mat from pylon image

            cvtColor(cv_img, image32f_1, COLOR_BGR2GRAY);           //Conver to BGR type
            Buffer[counter] = cv_img;                               //Place captured image into buffer
            //Begin implementation of EVM-------------------------
            //Spatial filtering
            pyrDown(Buffer[counter], Buffer[counter]);              //4 level Gaussian Pyramid
```

```
58              pyrDown(Buffer[counter], Buffer[counter]);
59              pyrDown(Buffer[counter], Buffer[counter]);
60              pyrDown(Buffer[counter], Buffer[counter]);
61              Buffer1[counter] = Buffer[counter];                  //Reduces image
     size and blurs image
62              //-----------------------------------------------------
63
64              if (counter1 == 1)                                  //If the image
    buffer s filled for the first time start outputting, and loop array back around

65              {
66                  Mat f_img = cv::Mat(Buffer[counter].rows*Buffer[counter].cols,
    WINDOW, CV_32F);     //columns contain rows and columns of each image stacked t
    ogether
67                  //Row of temp structure contain each image
68
                        //Perform Temporall FFT after buffer is filled
69                  for (int k = 0; k < WINDOW - 1; k++)
70                  {
71
72                      for (int j = 0; j < Buffer[k].cols; j++)
73                      {
74
75                          for (int i = 0; i < Buffer[k].rows; i++)
76                          {
77
78                              float *input = (float*)(Buffer[k].data);        //P
    oint to captured image
79                              float *output = (float*)(f_img.data);           //P
    oint to output image
80                              output[j*Buffer[k].cols + i, k] = input[j, i];//Sta
    ck rows and columns of image side by side
81                          }
82                      }
83                  }
84
85                  //FFT opencv example adaption
86                  Mat padded;                             //expand input image to
    optimal size
87                  int m = getOptimalDFTSize(f_img.rows);
88                  int n = getOptimalDFTSize(f_img.cols); // on the border add zer
    o values
89                  copyMakeBorder(f_img, padded, 0, m - f_img.rows, 0, n - f_img.c
    ols, BORDER_CONSTANT, Scalar::all(0));
90
91                  Mat planes[] = { Mat_<float>(padded), Mat::zeros(padded.size(),
     CV_32F) };
92                  Mat complexI = f_img;
93                  merge(planes, 2, f_img);         // Add to the expanded another
     plane with zeros
94
95                  Mat mask;
96                  dft(f_img, f_img, DFT_ROWS);        //Perform a dft along the r
    ows of the image to determine temporal frequencies
97
98
99                  split(complexI, planes);                    // planes[0] = Re(DF
    T(I), planes[1] = Im(DFT(I))
100                 magnitude(planes[0], planes[1], planes[0]);// planes[0] = magni
    tude
101                 Mat magI = planes[0];
102
```

```
103                 magI += Scalar::all(1);                    // switch to logarit
    hmic scale
104                 log(magI, magI);
105
106                 // crop the spectrum, if it has an odd number of rows or column
    s
107                 magI = magI(Rect(0, 0, magI.cols & -2, magI.rows & -2));
108
109                 // rearrange the quadrants of Fourier image  so that the origin
     is at the image center
110                 int cx = magI.cols / 2;
111                 int cy = magI.rows / 2;
112
113                 Mat q0(magI, Rect(0, 0, cx, cy));   // Top-
    Left - Create a ROI per quadrant
114                 Mat q1(magI, Rect(cx, 0, cx, cy));  // Top-Right
115                 Mat q2(magI, Rect(0, cy, cx, cy));  // Bottom-Left
116                 Mat q3(magI, Rect(cx, cy, cx, cy)); // Bottom-Right
117
118                 Mat tmp;                            // swap quadrants (Top-
    Left with Bottom-Right)
119                 q0.copyTo(tmp);
120                 q3.copyTo(q0);
121                 tmp.copyTo(q3);
122
123                 q1.copyTo(tmp);                     // swap quadrant (Top-
    Right with Bottom-Left)
124                 q2.copyTo(q1);
125                 tmp.copyTo(q2);
126
127                 normalize(magI, magI, 0, 1, CV_MINMAX); // Transform the matrix
     with float values into a
128
129                                                     // viewable image form
    (float between values 0 and 1).
130
131                 //Simple high pass butterworth 2d filter created by Matlab
132                 Mat kernel = (Mat_<double>(5, 5) << 0, 0, 0, 0, 0, 0, 0.0605, 0
    .1210, 0.0605, 0, 0, 0.1210, 0.4158, 0.1210, 0, 0, 0.0605, 0.1210, 0.0605, 0, 0
    , 0, 0, 0, 0); //kernel gereated by matlab
133
134
                    //Higher Degree Kernel
135
136
                    /*   0.0021    0.0084    0.0125    0.0084    0.0021
137
                    0.0084    0.0610    0.1053    0.0610    0.0084
138
                    0.0125    0.1053    0.2276    0.1053    0.0125
139
                    0.0084    0.0610    0.1053    0.0610    0.0084
140
                    0.0021    0.0084    0.0125    0.0084    0.0021 */
141 //cvtColor(kernel, kernel, CV_32F);
142                 //Apply desired bandpass filter
```

```
143                 filter2D(magI, magI, CV_32F, kernel, Point(-1, -
    1), 0, BORDER_DEFAULT);
144                 Mat magA = magI.mul(100);       //Amplify filter out put to amp
    lify temporal frequency band
145
146                 idft(magI, magI, DFT_ROWS);     //Inverse Fourier transsform
147
148
149
150                 for (int k = 0; k < WINDOW - 1; k++)
151                 {
152
153                     for (int j = 0; j < Buffer[k].cols; j++)
154                     {
155
156                         for (int i = 0; i < Buffer[k].rows; i++)
157                         {
158
159                             float *input = (float*)(magI.data);  //Pointer to f
    iltered output
160                             float *output = (float*)(Buffer1[k].data);  //place
     image row and column stacks in the right order to reconstruct images
161
162                             output[j, i] = input[j*Buffer1[k].cols + i, k];
163
164
165
166                         }
167
168
169                     }
170
171                 }
172
173
174
175
176
177                 pyrUp(Buffer1[counter], Buffer1[counter]);          //Upsample
    and move output up Gaussian Pyramid
178                 pyrUp(Buffer1[counter], Buffer1[counter]);
179                 pyrUp(Buffer1[counter], Buffer1[counter]);
180                 pyrUp(Buffer1[counter], Buffer1[counter]);
181                 Mat A = cv_img + Buffer1[counter].mul(40);          //Add Origi
    nal Images to image output
182                 imshow("Preview", A);
183
184             }
185             //-----------------------------------------------------------------
    -------------
186
187             waitKey(1);
188
189             //image32f_1.convertTo(Buffer[counter], CV_8U);
190             if (counter1 == 0)
191             {
192                 imshow("Preview", Buffer[counter]);
193
194                 waitKey(1);
195             }
196
197             counter++;
198             if (counter > WINDOW - 1)
```

```
199             {
200                 counter = 0;
201                 counter1 = 1;
202             }
203 
204         }
205         else
206         {
207             throw RUNTIME_EXCEPTION("Error image grab failed: %hs", ptrGrabResu
    lt->GetErrorDescription().c_str());
208         }           //Error Handling
209 
210 
211     } while (camera.IsGrabbing() && !yes);
212 
213     yes = 0;
214 
215 
216 }
217 catch (const GenericException &e)
218 {
219     // Error handling.
220     cerr << "An exception occurred." << endl
221         << e.GetDescription() << endl;
222 
223     cerr << endl << "Press Enter to exit." << endl;
224     while (cin.get() != '\n');
225 }
226 
```

Appendix II

Vein Visualisation Tool V.1.0 User Manual

Vein Visualisation Tool V1.0

User Manual

Installation Procedure and First Use

The Vein Visualisation Tool is designed to be used with a Basler ACE usb 3.0 camera. It may work with other Basler brand cameras but no testing or attempt to verify other camera models has been conducted.

The programme has been developed in c++, the Microsoft .Net framework must be installed in order to successfully run and install the program. Open Source Computer Vision (OpenCv) was used to handle and process images and version 3.0 or higher must be installed in order to run the application.

The software can be found at the following URL at the time of writing:

https://sourceforge.net/projects/opencvlibrary/files/opencv-win/3.1.0/opencv-3.1.0.exe/download

If all the requirements are met the program can be run from the VeinVisualisation.exe file and the program main screen should open.

Overview

The main application screen is shown below in Figure 1.

Figure 1.Vein Visualisation Main Screen

It allows the user to fully control the camera parameters and settings and is capable of demonstrating in real time every function of the vein visualisation device.

Figure 2. Main sections of interest in the programme window

The camera parameters can be set in the camera parameters section. Full control over the fps, exposure, width and height of captured video is given to the user along with the ability to set up the form of the output video.

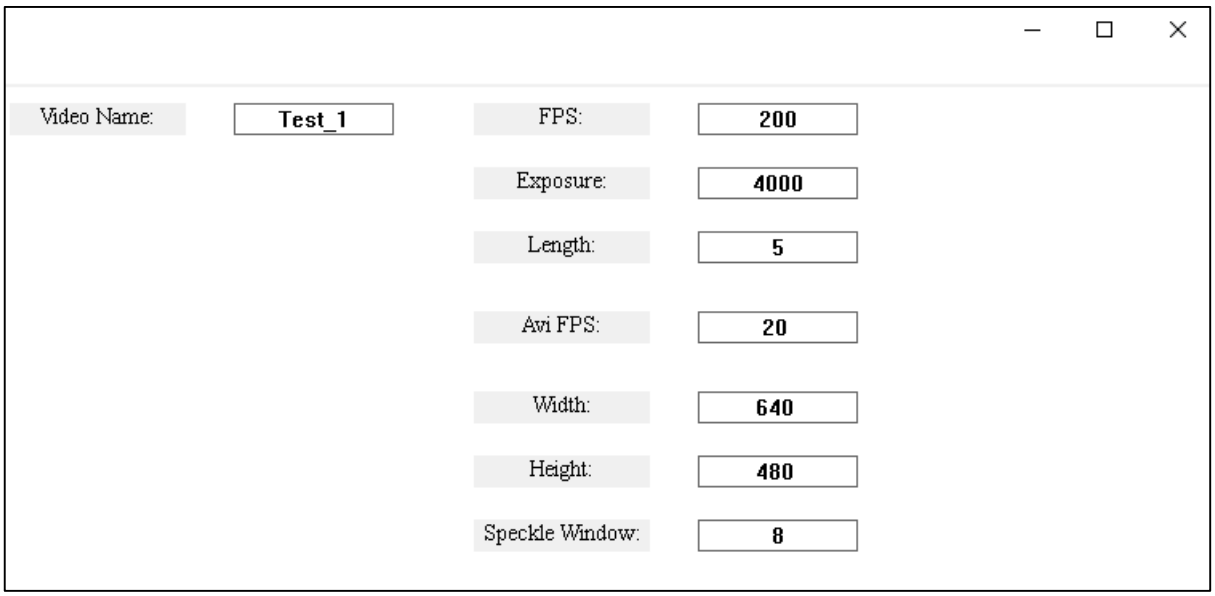

Figure 3. Camera setup screen

Setting the Frame Rate

The camera 'FPS' field, set to 200 by default, will prevent the camera from exceeding the specified framerate and where possible ensure that the camera operates at the specified value. Different cameras within the Basler ACE product line are limited at different framerates so it is important to ensure that the specified value can be achieved by the camera.

Setting the Exposure

The exposure setting is specified in microseconds eg a value of 1000 will correspond to a 1 ms exposure time. The minimum value is 59 ms. It is important to note that the exposure time will effect the maximum exposure achievable.

Setting the Length

The recording time is specified in seconds. The number of frames recorded is equal to the frame rate multiplied by the video length parameter.

Setting the Avi FPS

Specifies the playback rate of the video on a Windows machine, does not effect the number of frames recorded by the video.

Setting the width and height

The width and height can be specified. The maximum values set will be determined by the exact model of Basler camera and the product technical specifications should be consulted.

Setting the Speckle Window

This parameter is only used during acquisition using the 'Speckle' button and determines the window used to apply the LaSca algorithm.

Setting the Video Name

The video name, specifies what the recorded video will be named. The video will be recorded as an uncompressed avi file.

Registering changes:

When the parameters have been set it is important to press the 'set' button in order to register the changes. It is important, if a recording or image preview operation has been started that the end preview button is pressed before setting the camera settings.

Recording a Video

In order to record a video, set the camera parameters as described. The 'Preview' button can be used to align the camera and ensure that the frame is set up properly. When everything is set up correctly press the 'end preview' button and press the 'Record' button. Recording will stop after the specified period of time, the output will be stored within the installation folder and named as specified in the video name

edit box. It is important to note that any existing file of the same name will be overwritten by the new file.

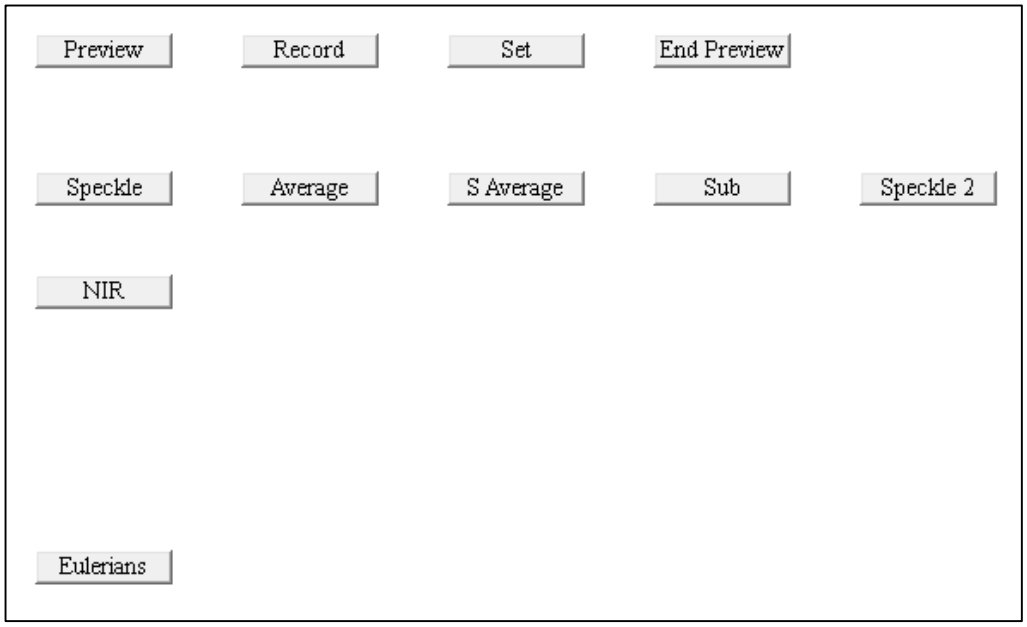

Figure 4. The preview and record section of the vein visualisation tool

Previewing Camera Output and Performing Image Processing Operations

The remaininng buttons all perform a variety of image processing operations. The ‘Speckle’ button calculates the speckle contrast of each image and displays the output in real time. It divides the image into n x n sub elements determined by the window setting in the parameter section.

Laser Speckle Imaging Operations

“Speckle”

The mean and standard deviation of each window are calculated and the speckle contrast is determined for each window from the following equation.

$$K = \frac{\widehat{I_{nn}}}{\sigma_{nn}}$$

Typically this is used to determine dynamic movement of a speckle field.

“Average”

This button outputs the average intensity value of each image pixel over a 50 image window. Output will not begin until the fifty image buffer is filled, after which point, every image displayed will represent the moving window average of the last 50 images.

"SAverage"

This button calculates the speckle contrast of each image as described within the Speckle algorithm description. The output is stored in a rolling average and the average of the last 50 speckle images is displayed. Spatial and temporal features of the speckle field can be observed through this setting.

"Sub"

This button outputs the result of subtracting the last image captured from the current image. The difference image is displayed.

Near Infrared Imaging Operations

"NIR"

This button uses adaptive histogram equalisation to maximise the image contrast. The high contrast image is then sharpened using high frequency filter operations and the result is output to the screen.

The high pass 2d butterworth filter is applied to the image with the flter mask shown below:

$$h = \begin{matrix} 0.0271 & 0.1082 & 0.1623 & 0.1082 & 0.0271 \\ 0.1082 & -0.4328 & -1.0821 & -0.4328 & 0.1082 \\ 0.1623 & -1.0821 & 4.4367 & -1.0821 & 0.1623 \\ 0.1082 & -0.4328 & -1.0821 & -0.4328 & 0.1082 \\ 0.0271 & 0.1082 & 0.1623 & 0.1082 & 0.0271 \end{matrix}$$

Where h is the spatial image filter mask.

Eulerian Video Magnification

This button implements a near-real time adaption of the video processing method outlined by Michael Rubenstein and a team at MIT. The link to there work is shown below.

http://people.csail.mit.edu/mrub/vidmag/

It aplifies temporal frequencies corresponding to heart rate. It masses an image buffer of 2 seconds of video captured at 20 fps. (The fps setting is set automatically) . The temporal

frequencies are extracted using a band pass filter and amplified. They are then placed back on the original video to visualise heart rate and movement.

Vein Visualisation Testing Software V.1.0 User Manual

Vein Visualisation Testing Software V1.0 User Manual

Installation Procedure and First Use

The Vein Visualisation testing software is written using the Matlab runtime environment. It is designed to be used to perform a number of tests which are capable of evaluating a system built during the completion of an ME in Biomedical Engineering project entitled "Developing a non-contact Vein Visualisation and Heart Rate Monitoring Device".

To install the programme open up the folder containing the packaged software. In the root directory double click on the file the vein visualizer as illustrated in figure 1.

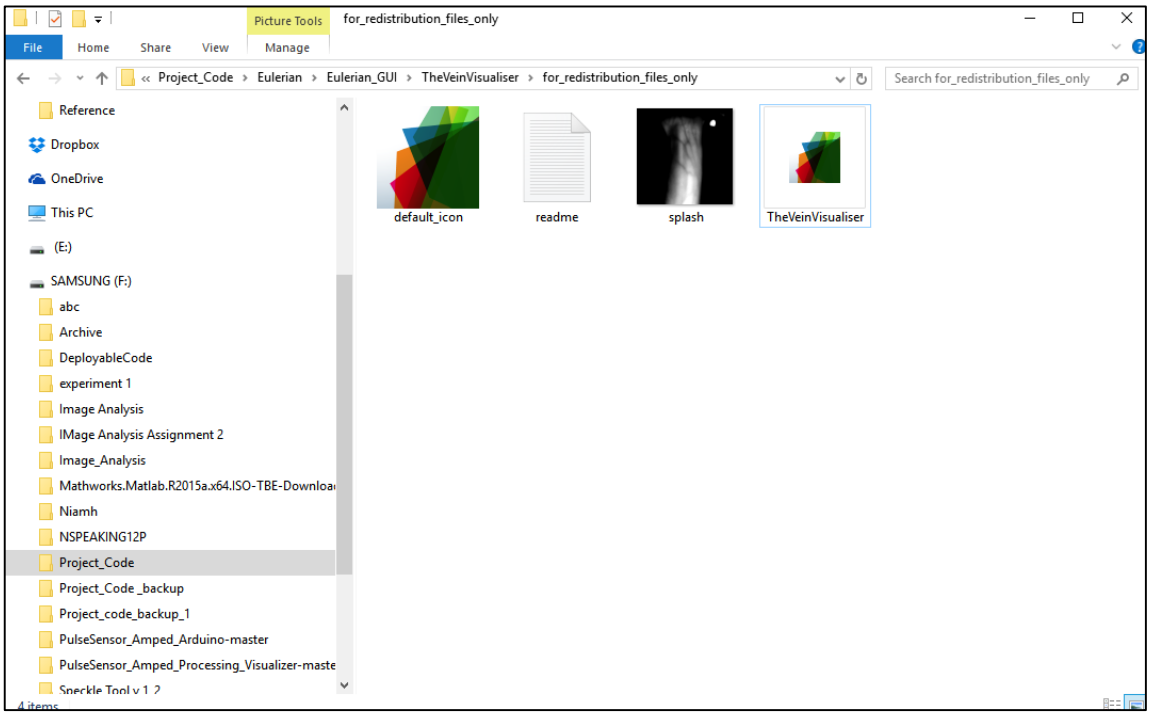

Figure 1. Installing the application

If Matlab runtime v.8.5 is not installed a screen will appear and guide the user through the installation process. The installation screen will then appear to guide the user through installation. Clicking next will begin the installation procedure.

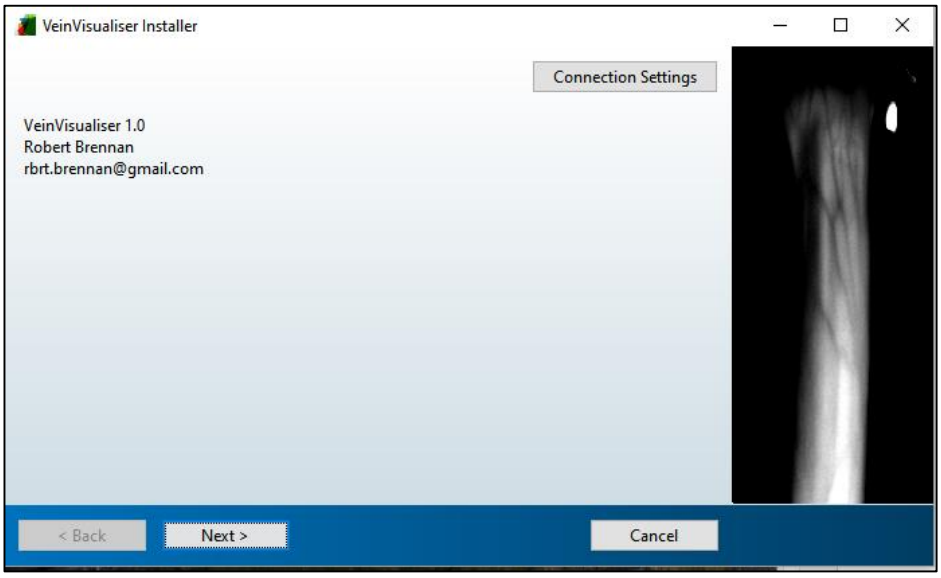

Figure 2. Installation Screen

The installation directory can be set and if desired a shortcut can be placed on the computers desktop.

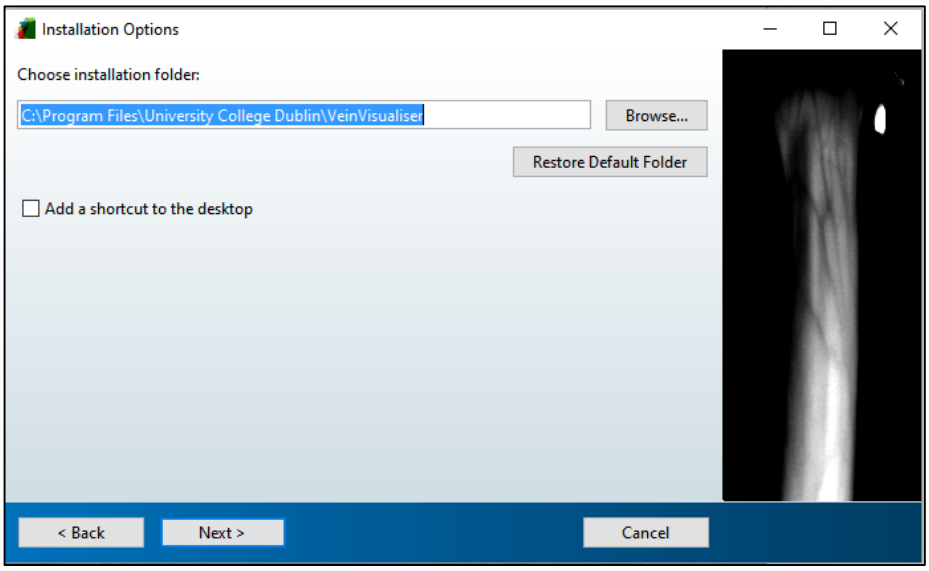

Figure 3.Selecting the installation directory

Clicking next again will install the program. After the installation completes the window will close indicating a successful installation. To run the programme simply locate the veinvisualisation.exe file within the installation direction or open the shortcut created on the desktop.

Overview

The main application screen is shown in figure 4. It can be divided into three distinct regions which perform the individual tests.

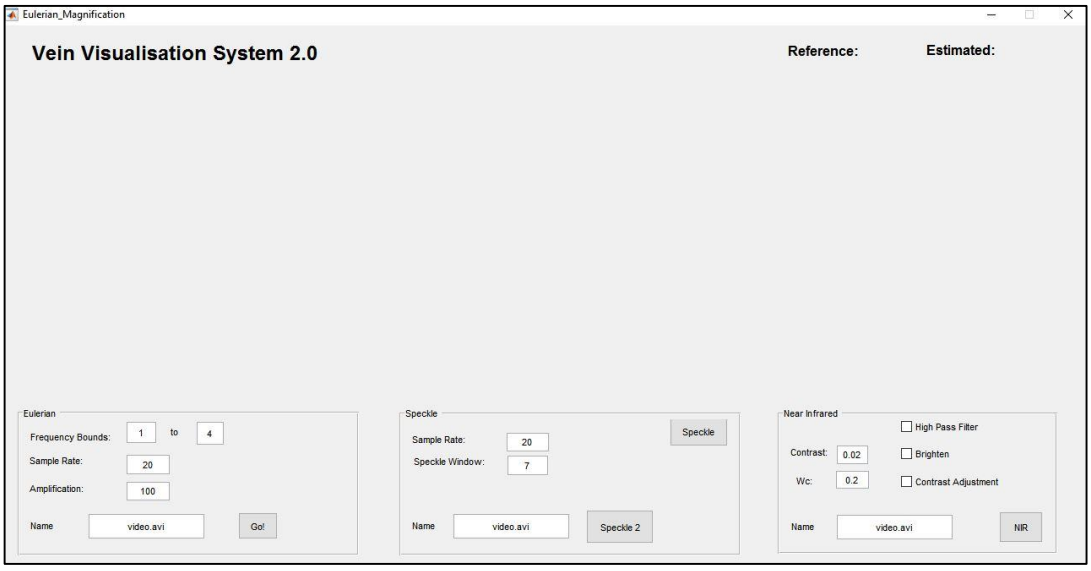

Figure 4.The three panels each control the settings for three testing procedures

Three tests can be run using the application. Each test is contained within each of the three panels. The three testing procedures are described in depth in each section.

Eulerian Video Magnification

The Eulerian panel allows Eulerian magnification to be tested and used to extract heart rate from videos. It applies the algorithm developed in a MIT research project, a link to the original work is provided below:

http://people.csail.mit.edu/mrub/vidmag/

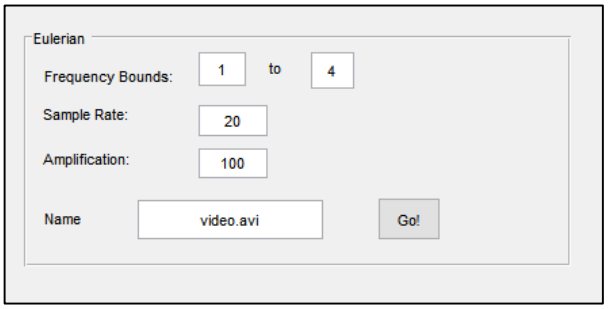

Figure 5.Parameter specification for Eulerian Video Magnification Test

Figure 5 illustrates the parameter selection box. Before initiating the test parameters must be chosen. The frequency bounds specify the frequency band in Hz which will be amplified within the generated output. To test heart rate typically .5 Hz to 4 Hz are selected to represent the full range of possible heart rates. The video will be less prone to error when a smaller frequency band is chosen. The sample rate selected should be the frame rate of the captured video. The level of amplification of the specified frequency can also be selected, higher values will produce a more exaggerated impression of the movements occurring within the specified frequency band. Finally the video name and filename have to be specified. The go button will initiate the testing procedure.

A cursor will appear prompting the user to select a point on the users skin from which heart rate will be estimated. Clicking the mouse will confirm the point.

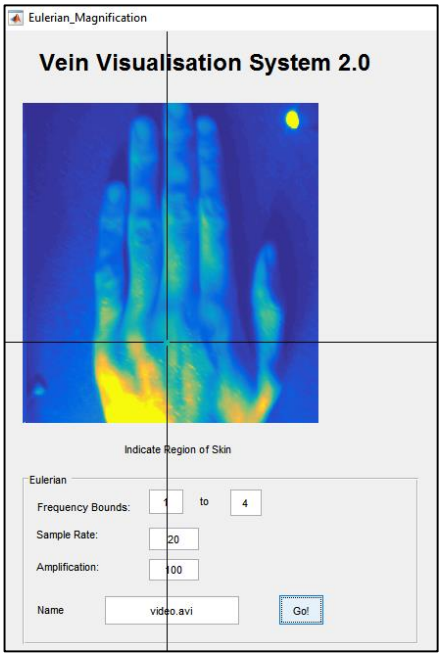

Figure 6.Selecting a point on the users skin

The user will similarly be prompted to select a point indicating the heart rate indicator.

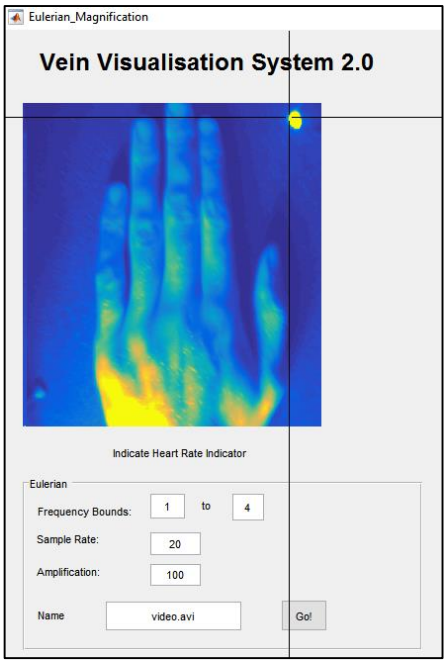

Figure 7.Indicating the heart rate indicator

After a short delay the two selected regions will be mapped onto the output video and the real-time video enhancement will be presented. The mean squared value of the skin and indicator regions will be mapped as the video is processed.

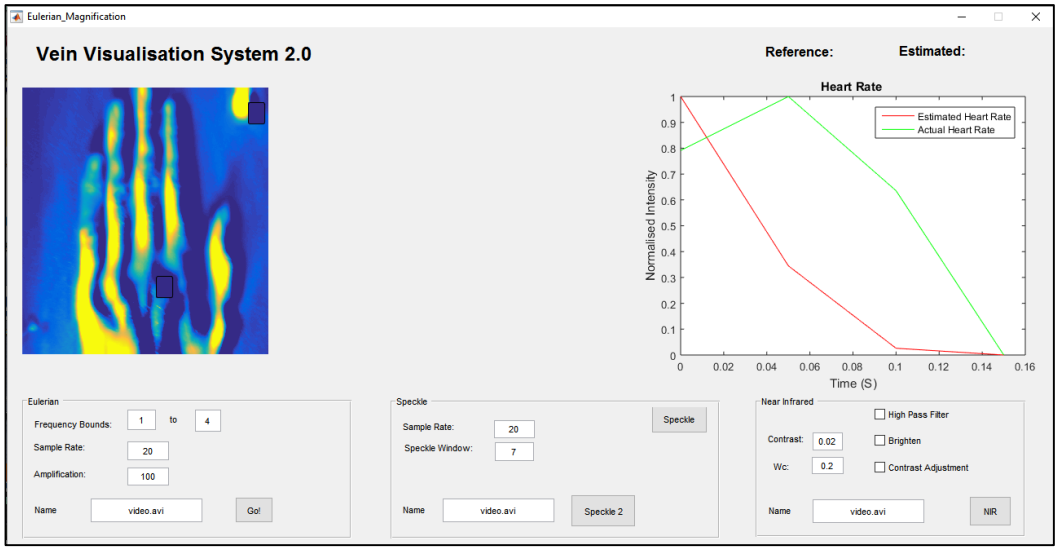

Figure 8. Performing Eulerian Video Magnification

When the video has finished the number of intensity peaks are automatically counted and output to the screen for both the actual heart rate and estimated signal. The number of beats for each of the signals will be displayed above the plotted graph. The video output will be written to the installation directory

The following naming convention is used "{videotitle}.avi-{low frequency}hz-to-{high frequency}hz -alpha-{amplification}.avi".

Speckle Imaging

To apply the LaSCA algorithm to the video input the second panel is used to set up algorithm parameters.

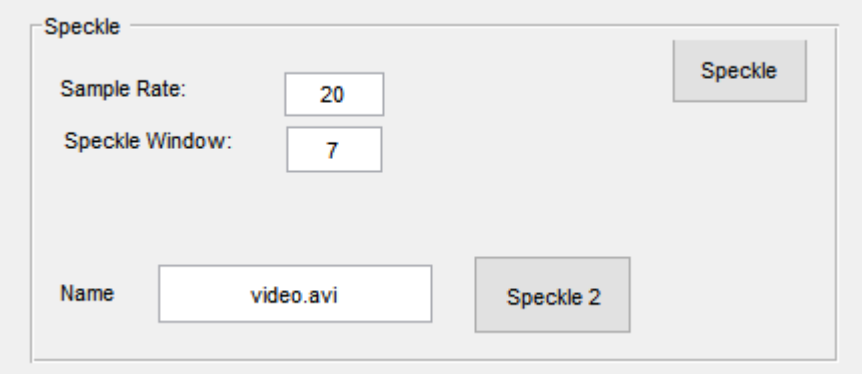

Figure 9. Laser Speckle Parameter Selection

The input video frame rate is input into the sample rate field. The size of the speckle window determines the size of the sub elements that the image is divided into. Larger windows reduce the spatial resolution but to prevent signal corruption the size specified must be twice as large as the calculated speckle size. When the speckle button is pressed the user will be prompted to select a point indicating the top left of the speckle field and then the bottom right of the speckle field.

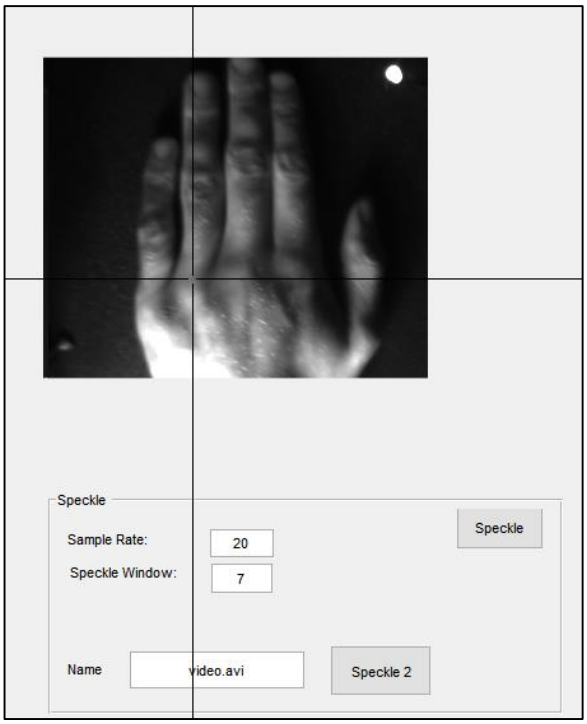

Figure 10. Determining the region filled by the speckle pattern

When the region of interest has been selected the processing will readjust so that the box region fills the output screen. The LaSca algorithm will be applied and the speckle contrast map will be output to the screen.

Two preview windows will be displayed. The output on the left displays the averaged output of the LaSCA algorithm over a rolling 20 frame window. The frame on the right displays the raw output of the LaSCA algorithm. The video is output to the installation folder under the following naming convention: {videotitle}.avi-Speckle-1{timestamp}.

NIR Enhancement

The third function is used to enhance the contrast and clarity of vein images captured using the vein visualisation system.

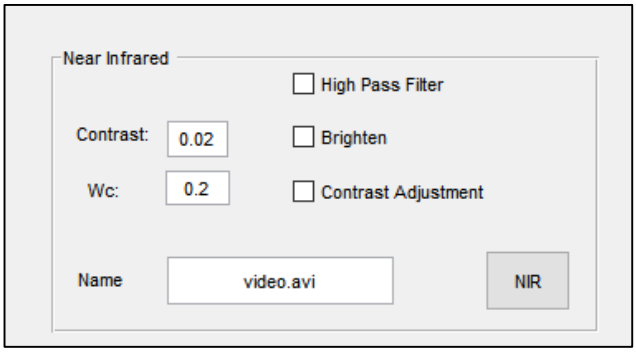

Figure 11. NIR enhancement parameters

The level of contrast adjustment is selected in the contrast input field. Wc determines the frequency cut off point which determines the level of sharpening. The check boxes select the enhancement operations which are applied to the video.

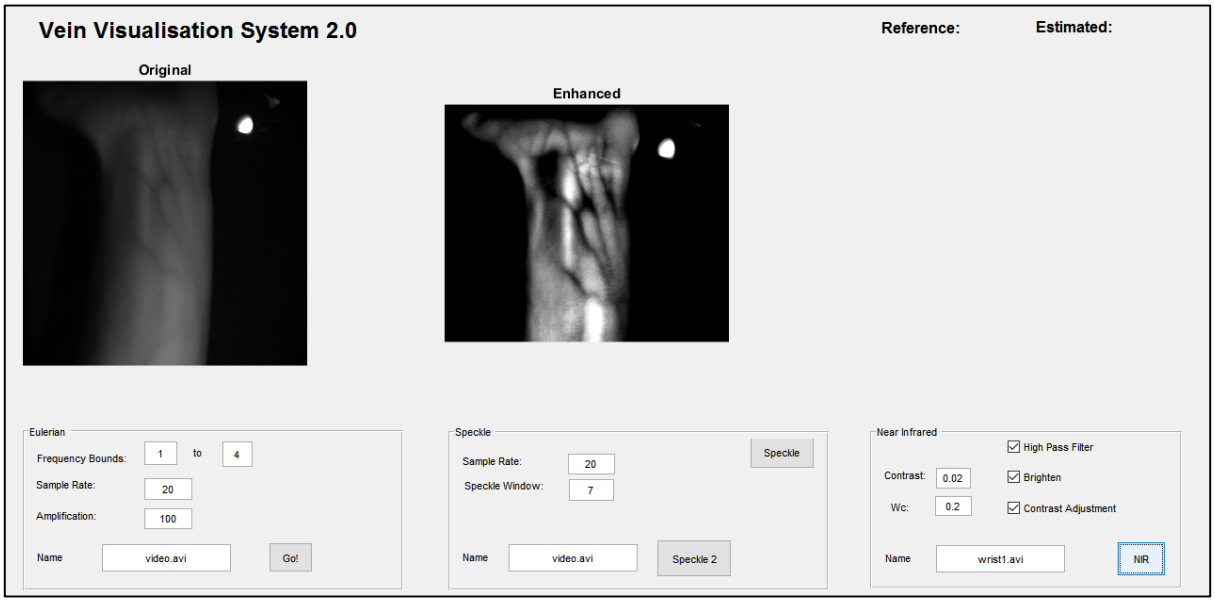

Figure 12. Illustration of NIR image enhancement

The output is written to the installation directory using the following naming convention: {video name}-NIR-{timestamp}.avi